Protistan plankton communities in the Galápagos Archipelago respond to changes in deep water masses resulting from the 2015/16 El Niño

Erika F. Neave[1,2,3] (e.neave@nhm.ac.uk), Harvey Seim[1] (hseim@email.unc.edu), Scott Gifford[1] (sgifford@email.unc.edu), Olivia Torano[1] (omtorano@email.unc.edu), Zackary I. Johnson[4] (Zackary.johnson@duke.edu), Diego Páez-Rosas[5] (dpaez@usfq.edu.ec) and Adrian Marchetti[1*]

Affiliations:

[1] Department of Marine Sciences, University of North Carolina at Chapel Hill, Chapel Hill, NC, USA

[2] Present address: Department of Life Sciences, Natural History Museum, London, UK

[3] Present address: School of Biological and Environmental Sciences, Liverpool John Moores University, Liverpool, UK

[4] Marine Laboratory and Biology Department, Duke University, Beaufort, NC, USA

[5] Galápagos Science Center, Universidad San Francisco de Quito, Isla San Cristóbal, Islas Galápagos, Ecuador

***For correspondence:**

Dr. Adrian Marchetti

Department of Marine Sciences

University of North Carolina at Chapel Hill

3202 Venable Murray Hall CB 3300

Chapel Hill, NC 27599-3300, USA

Email: amarchetti@unc.edu

Tel. (+1) 919 843 3473

Fax (+1) 919 962 1254

Author Contributions:

E.F.N – study conception, data acquisition, data analysis, draft manuscript, approved manuscript

H.S. – data acquisition, data analysis, draft manuscript, approved manuscript

S.G. – draft manuscript, approved manuscript

O.T. – data acquisition, approved manuscript

Z.I.J – data acquisition, approved manuscript

D.P-R. – data acquisition, approved manuscript

A.M. – study conception, data acquisition, data analysis, draft manuscript, approved manuscript

ORCIDs:

E.F.N: 0000-0002-0410-0338

H.S: 0000-0002-1562-0849

S.G: 0000-0002-3222-9681

Z.I.J.: 0000-0003-0793-8512

D.P-R: 0000-0002-2446-9888

A.M: 0000-0003-4608-4775

Conflict of interest

The authors declare that they have no conflict of interest.

Abstract

The Galápagos Archipelago lies within the eastern equatorial Pacific Ocean at the convergence of major ocean currents that are subject to changes in circulation. The nutrient-rich Equatorial Undercurrent upwells from the west onto the Galápagos platform, stimulating primary production, but this source of deep water weakens during El Niño events. From measurements collected on repeat cruises, the 2015/16 El Niño was associated with declines in phytoplankton biomass at most sites throughout the archipelago and reduced utilization of nitrate, particularly in large-sized phytoplankton in the western region. Protistan assemblages were identified by sequencing the V4 region of the 18S rRNA gene. Dinoflagellates, chlorophytes, and diatoms dominated most sites. Shifts in dinoflagellate communities were most apparent between the years; parasitic dinoflagellates, *Syndiniales*, were highly detected during the El Niño (2015) while the dinoflagellate genus, *Gyrodinium* dominated many sites during the neutral period (2016). Variations in protistan communities were most strongly correlated with changes in subthermocline water density. These findings indicate that marine protistan communities in this region are regimented by deep water mass sources and thus could be profoundly affected by altered ocean circulation.

Introduction

The Galápagos Archipelago and surrounding waters (1-2 °S, 90-92 °W) are renowned for having diverse, highly productive ecosystems. The need to protect their marine ecosystems led to the establishment of the Galápagos Marine Reserve (GMR) in 1998 (Bensted-Smith, 1998). Despite greater efforts to conserve and study the GMR, one of the main sources of primary production, the marine protists, remain largely understudied. Protistan plankton exhibit diverse trophic modes, ranging from autotrophic phytoplankton to heterotrophic flagellates. A shift in protist community composition can therefore drastically alter the quantity of food available for higher trophic levels, and thus influence the overall productivity of the Galápagos marine ecosystem (De Vargas *et al.*, 2015).

The convergence of ocean currents allows waters within the archipelago to have high primary production relative to the surrounding Eastern Equatorial Pacific (EEP) Ocean, a region considered high-nutrient, low-chlorophyll. The EEP is a high-nutrient, low chlorophyll region due to iron limitation (Behrenfeld *et al.*, 1996), which is largely relieved in the GMR when currents upwell lithogenic nutrients from the Galápagos platform (Barber and Chavez, 1991; Rafter, Sigman and Mackey, 2017). Three major ocean currents provide the bulk of nutrient sources to the region (Lindley and Barber, 1998; Fiedler and Talley, 2006). The South Equatorial Current flows westward, enveloping the equator, and is fed by the Peruvian coastal upwelling and equatorial upwelling (Pennington *et al.*, 2006) (Figure 1a). The North Equatorial Countercurrent flows eastward, transporting western Pacific warm pool water to the north of the South Equatorial Current. The most critical supply of nutrients to the region comes from the eastward-flowing Equatorial Undercurrent (EUC) which collides subsurface with the western side of the Galápagos platform. It flows around and through the archipelago below the surface

93 layer (Kessler, 2006) carrying nutrient rich subtropical underwater, and can outcrop west of the
94 archipelago, making this region a primary productivity hotspot (Chavez and Brusca, 1991;
95 Sakamoto *et al.*, 1998).

96 Marine protistan communities in the EEP are influenced by El Niño Southern Oscillation
97 (ENSO), a spatio-temporally complex interannual shift in equatorial Pacific Ocean circulation.
98 The EEP harbors mostly small-sized phytoplankton communities consisting of *Prochlorococcus*,
99 *Synechococcus*, and picoeukaryotes (Chavez *et al.*, 1996). However, when equatorial upwelling
100 is strong it can provide sufficient iron and silica for large-sized phytoplankton such as diatoms to
101 bloom (Pennington *et al.*, 2006; Masotti *et al.*, 2010; Marchetti *et al.*, 2010). During an El Niño
102 event, EEP sea surface temperatures (SST) rise above the climatological average causing
103 stratification. This results in weaker equatorial upwelling, a deeper thermocline, and a slower
104 EUC. El Niño conditions lead to reduced nitrate availability and decreases in *Synechococcus*,
105 likely because of their high cellular nitrogen requirement (Moore *et al.*, 2002), which allow small
106 heterotrophic protists to dominate, altering marine food web dynamics in the EEP (Masotti *et al.*,
107 2010). Contrary to community dynamics in the EEP, on the west side of the Galápagos
108 Archipelago, *Synechococcus* and *Prochlorococcus* concentrations decreased during a neutral
109 period of stronger upwelling following the 2015/16 El Niño (Gifford *et al.*, 2020). Given that
110 *Prochlorococcus* is speculated to prefer nitrogen sources other than nitrate, it may be more
111 competitive under stratified El Niño conditions (Moore *et al.*, 2002). There is less understanding
112 of how shifts in photosynthetic eukaryotes and other protists are influenced by ENSO in the
113 Galápagos Archipelago specifically, where increased vertical mixing allows for a relatively
114 higher baseline phytoplankton biomass than the surrounding EEP (Barber *et al.*, 1996).

Despite limited knowledge on protistan communities, establishing causes for fluctuations in phytoplankton biomass in the GMR has been investigated previously (Maxwell, 1975; Feldman, 1986). Some studies have used satellite chlorophyll *a* (Chl *a*) proxies to understand phytoplankton biomass variability (Liu *et al.*, 2014; Kislik *et al.*, 2017). Despite seasonal Chl *a* variability in the GMR, its amplitude varies with basin-scale SST trends, in that Chl *a* peaks in the Boreal spring, synchronous with the strengthening of the EUC (Palacios, 2004; Sweet *et al.*, 2007). However, this temporal pattern in Chl *a* amplitude does not hold true spatially, as individual bioregions of the GMR differ (Edgar *et al.*, 2004). The South Equatorial Current and the North Equatorial Countercurrent meet forming the equatorial front. The seasonal oscillation of this has been used to predict patterns of Chl *a* concentration (Schaeffer *et al.*, 2008). In the latter part of the year, the strengthening and tilt of the equatorial front can largely explain Chl *a* variability (Palacios, 2004).

Fewer studies have focused on observing in situ environmental conditions and their influence on protistan community compositional changes (McCulloch, 2011; Carnicer *et al.*, 2019). These observations are necessary for understanding the ecological implications of El Niño events in this region. Sporadic surveys of phytoplankton communities provide a historical record of common diatoms and dinoflagellate species, however they are limited to observations of large, more “charismatic” species easily identified using light microscopy (Torres, 1998; Torres and Tapia, 2000, 2002; Tapia and Naranjo, 2012). Some harmful algal species were identified along with spatial variability in dinoflagellate diversity, which was attributed to changes in deep water masses to the west of the Galápagos platform (Carnicer *et al.*, 2019). Accessory phytoplankton pigments have also been used to assess phytoplankton composition in the GMR, such that

relative abundances of diatoms and chlorophytes were found to decrease during the 2004/05 El Niño event, while cyanobacteria and haptophyte proportions increased (McCulloch, 2011).

In this study, DNA metabarcoding (i.e., sequencing the 18S rRNA [18S] gene) was used to examine protistan community composition. Here we show distinct shifts in protist plankton genera in waters of the Galápagos Archipelago and how they correlate with primary productivity and oceanographic variables during the 2015/16 ENSO cycle. Because protistan plankton are important links between oceanographic processes and marine food webs, it is imperative to understand factors influencing their composition and production with shifts in environmental conditions attributed to climatic events.

Methods and materials

Sample collection

Fifteen sites within the GMR (89 – 92 ºW, 1.5 ºS – 2 ºN) were sampled over October 10th to 24th of 2015 and October 19th to November 11th of 2016 (Figure 1a). Based on the Oceanic Niño Index and the location of the GMR, situated within both the Niño 1.2 region (80 – 90 ºW, 0 – 10 ºS) and the Niño 3 region (150 – 90 ºW, 5 ºN – 5 ºS), our sampling periods occurred during El Niño (2015) and neutral conditions (2016) (Santoso, Mcphaden and Cai, 2017). Remote sensing of sea surface temperatures in the region indicate significantly warmer surface waters during the sampling period in 2015 relative to 2016 (Figure 1c-d). Using a Seabird SBE 19plus V2 SeaCAT Profiler, CTD profiles of temperature, salinity and photosynthetically active radiation (PAR) were collected to ~100 m depth. Ten liter Niskin bottles were used to collect seawater from the euphotic zone at 50%, 30%, 10%, and 1% incident irradiance (I_o) depths to measure dissolved inorganic nutrients, Chl *a*, dissolved inorganic carbon (DIC) and nitrate

(NO_3^-) uptake rates, and picoplankton cell counts. Seawater was dispensed into acid-cleaned, seawater rinsed 10 L Cubitainers (Hedwin Corporation, Newark, DE, USA) and subsampled for measurements. Additional seawater was collected from 50% I_o to obtain DNA (Figure 1a). Not all sites yielded DNA concentrations sufficient for sequencing. Processed filters and samples were frozen at -20 ºC until onshore analysis.

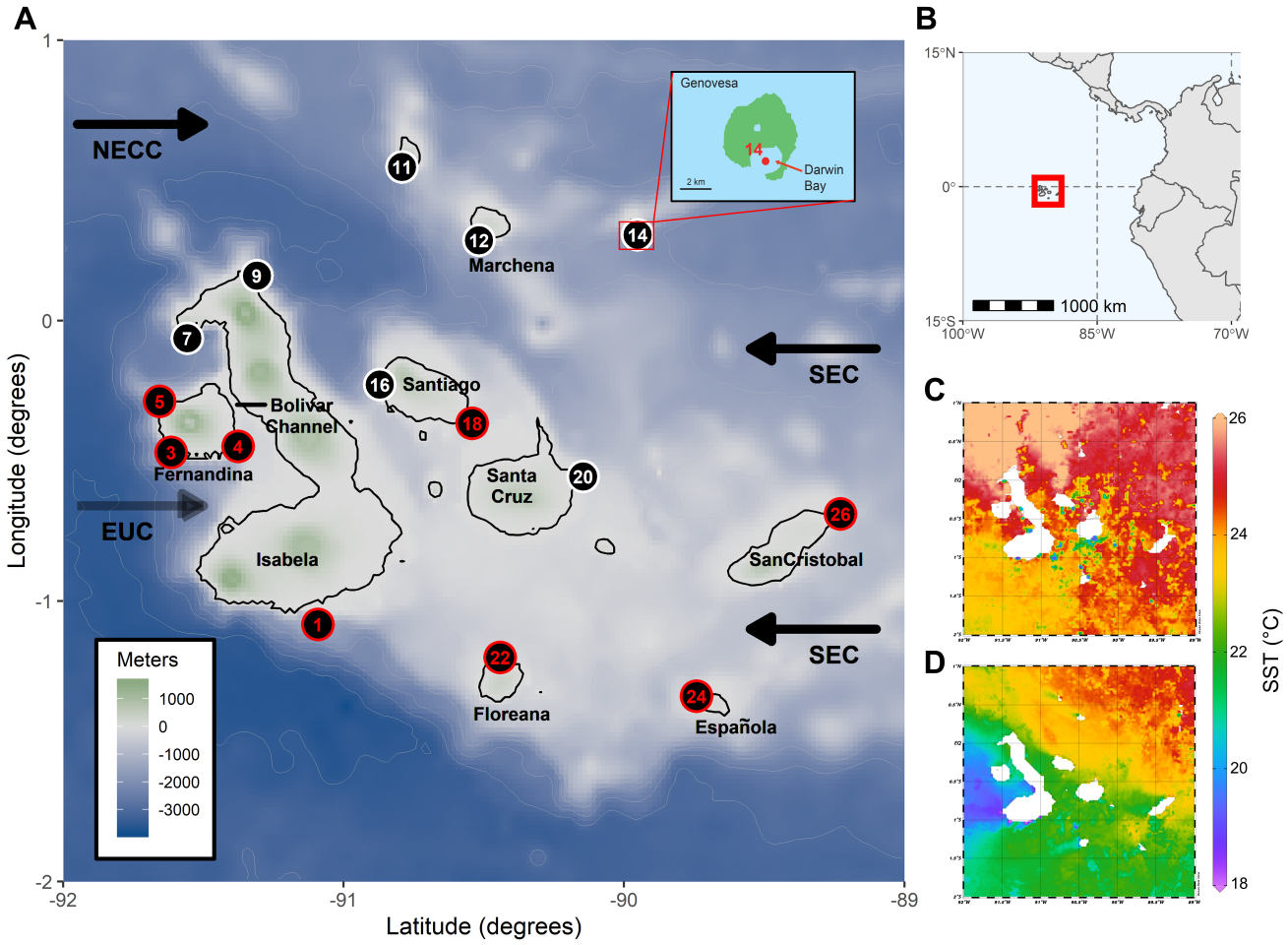

Figure 1.

The Galápagos Archipelago study region. A) Topographic map of the Galápagos Archipelago and sampling locations. White numbers indicate sites which were sampled for oceanographic measurements while red numbers indicate sites that were sampled for oceanographic measurements and protistan community DNA. Currents are abbreviated such that: SEC = South Equatorial Current, NECC = North Equatorial Countercurrent, and EUC = Equatorial Undercurrent. Upper right inset shows the location of site 14 near Genovesa Island, a partially collapsed caldera. B) Map showing the location of the Galápagos Archipelago within the Eastern Equatorial Pacific. Monthly averaged sea surface temperatures (NOAA AVHRR) throughout the Galápagos Archipelago for the sampling period in C) October of 2015 and D) October of 2016.

Seawater Properties

Temperature and salinity profiles were used to determine the depths of the mixed and subthermocline layers. All CTD casts were corrected using SeaBird's SeaSoft software. Potential density (hereafter referred to as 'density') was calculated using the sw_pden() function from the Mixing Oceanographic toolbox v 1.8.0.0 in MATLAB (R2017b). A consistent density structure was observed, of a surface and deep layer of almost uniform density, separated by a density gradient (interfacial layer) that was typically 10s of meters thick. The surface mixed layer depth was defined as the depth at which the change in density from the surface was > 0.35 kg/m^3. The subthermocline layer depth (the top of the deep layer of uniform density) was determined by calculating the depth at which change in density from the bottom of the cast was > 0.2 kg/m^3. The casts were visually inspected to ensure that the density cut-off values defined the layers

206 appropriately. Temperature, salinity, and density of the mixed and subthermocline layers were
207 averaged from CTD cast measurements. Methods for measuring dissolved inorganic nutrients are
208 described in the supplemental material.

209 **Phytoplankton Biomass and Productivity**

210 Phytoplankton biomass was approximated by measuring size-fractioned (<5 μm and >5
211 μm) Chl *a* concentrations using the acetone extraction method (Sartory and Grobbelaar, 1984).
212 Picophytoplankton cells, specifically *Prochlorococcus*, *Synechococcus*, and picoeukaryote
213 populations were enumerated using flow cytometry (Johnson *et al.*, 2010). Size-fractionated
214 DIC (i.e. primary productivity) and NO_3^- uptake rates were measured from 24 hr incubations
215 using stable isotope tracer techniques (Dugdale and Goering, 1967; Hama *et al.*, 1983).
216 Additional methods describing Chl *a*, flow cytometry, primary productivity and NO_3^- uptake
217 measurements are provided in the supplemental material.

218 **DNA sequencing and Bioinformatics**

219 Protistan taxonomic identification and proportions were obtained through sequencing the
220 V4 region of the 18S rRNA gene. DNA collection and amplicon library preparation are
221 described in the supplemental material. Approximately four million paired-end reads were
222 obtained using the Illumina MiSeq sequencing platform across two lanes. Mean amplicon length
223 for sequencing lane one was 561 bp, while mean amplicon length for sequencing lane two was
224 599 bp. Sequence files were demultiplexed. QIIME 2 v.2018.6 software was used for processing
225 the raw reads into assembled amplicons. The QIIME 2 plug-in, DADA2 was used for denoising
226 such that reverse and forward reads were truncated to 250 base pairs (bp) and 210 bp, and 260 bp
227 and 280 bp, for sequencing lanes one and two respectively. Chimeras were removed by the
228 consensus method and reads were merged (Supplementary Table 1) using default scripts

provided in the QIIME 2 documentation (docs.qiime2.org). Assembled amplicons were annotated by a BLAST search against the SILVA v. 123 reference database using a 90% pairwise identity cutoff. Metazoans were removed. Using the R package phyloseq v. 1.24.2, the samples were rarefied to 2066 reads per site (Supplementary Figure 1).

Annotations which were unknown in the highest taxonomic ranks (Kingdom, Phylum, Class, Order) were removed, under the assumption that it was unlikely to sample a novel high taxonomic rank of plankton. Custom taxonomy was assigned to the Class taxonomic rank based on the top seven relatively abundant groupings (Supplementary Table 2). Any annotation that did not belong to the top seven groups was annotated as "Other". Unknown or uncultured annotations in the lowest three taxonomic ranks (Family, Genus, Species) were grouped into the "Other" category within their respective Class ranks. Additionally, where possible, the top seven genera were maintained while the rest were also annotated as "Other" (there were only six known genera in the Chlorophyta). This resulted in 120 genera, prior to grouping unknown and uncultured OTUs (Supplementary table 2). All raw sequences have been deposited in the NCBI SRA database (Accession No. PRJNA689599).

Statistical Analyses

Analysis of water properties, phytoplankton biomass, productivity, and 18S data was performed using the vegan package (v. 2.5-4) in R version 3.6.2. Summary statistics and Mann-Whitney-Wilcoxon tests were used to test for differences in dissolved nutrients, Chl *a*, primary productivity and NO_3^- uptake rates between the two sampling years (Supplementary Table 3). The 18S data was arranged in an OTU table and transformed to relative proportions at the genus level, from which Bray-Curtis dissimilarity distances were calculated using the vegdist() function. All other variables (i.e., physical water properties, phytoplankton biomass, primary

252 productivity and NO_3^- uptake rates) were similarly transformed to Euclidean distances. A
253 correlation matrix was used to assess which variables were relatively redundant (Supplementary
254 Figure 2). These variables were removed for the BIO-ENV ('biota-environment') analysis. The
255 bioenv() function was used to find the best subset of variables which had the maximum rank
256 correlation with the community Bray-Curtis dissimilarities (Clarke and Ainsworth, 1993). These
257 variable subsets were identified for the entire protistan community and for the following
258 subgroups of the community: dinoflagellates, chlorophytes, and diatoms. A Non-metric Multi-
259 Dimensional Scaling (NMDS) plot was made from the Bray Curtis community dissimilarity
260 distances. The envfit() function was then used to fit the best subsets of variables onto the
261 community dissimilarity ordinations (Supplementary Table 4).
262
263 **Results and Discussion**
264 **Physical seawater properties**
265 Differences in upper ocean physical seawater properties between the El Niño (2015) and
266 neutral (2016) years were apparent (Figure 2, Supplementary Table 5). At most sites, mixed
267 layer depths were deeper in 2015 then 2016 (Fig. 2a). The mixed layer temperature range was
268 warmer in 2015 (22.9-26.4 ºC) relative to 2016 (17.1-23.7 ºC), with a mean difference of 3.8ºC
269 (Figure 2b). Mixed layer salinities varied by an average of 0.23 PSU, with most being higher in
270 2015 (Figure 2c). As a result, the mean density in 2016 was higher by 0.99 kg/m^3 during the
271 neutral period (Figure 2d). These differences in densities also existed spatially, such that the sites
272 located west of Isabela Island (Sites 3-7) had the highest mixed layer density values in 2016
273 (Figure 2d). Similar interannual density trends were observed in the subthermocline layer, where
274 subthermocline depths at most sites were deeper in 2015 than 2016 (Fig. 2e). The subthermocline

layer was on average 3.2 ºC cooler and 0.07 PSU fresher in 2016 resulting in seawater which was on average 0.70 kg/m^3 denser relative to the El Niño (Fig. 2f-h). One notable exception was site 14 located near Genovesa Island, inside a partially submerged caldera (see inset map in Fig. 1a). The caldera is isolated from surrounding ocean by an approximately 10 m deep sill, restricting exchange with waters outside the caldera and allowing seawater properties within the caldera to remain more constant between years. Aside from this site outlier, subthermocline layer densities showed consistent temporal change relative to the mixed layer, which was more spatially sensitive.

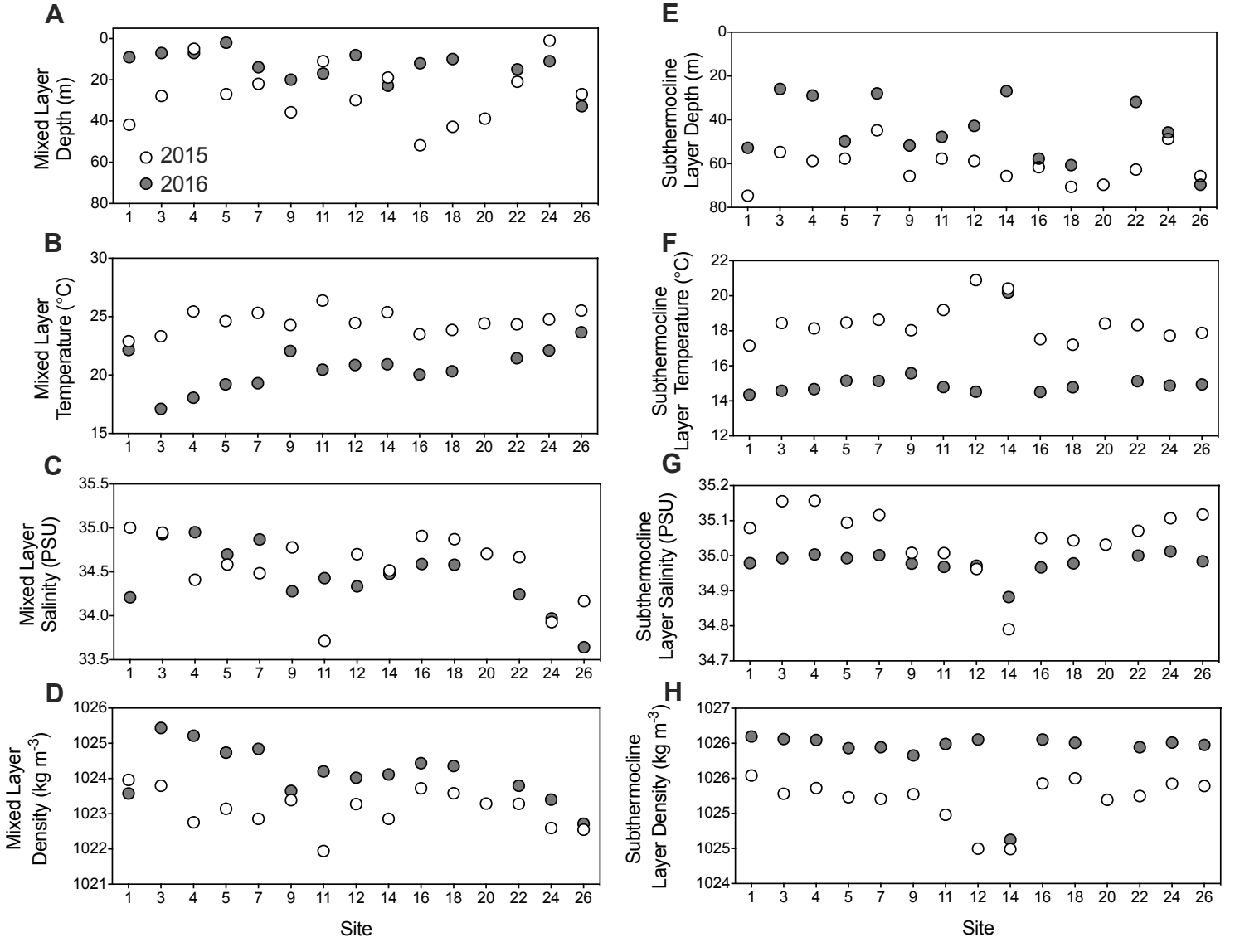
A
Mixed Layer Depth (m)
2015
2016
B
Mixed Layer Temperature (°C)
C
Mixed Layer Salinity (PSU)
D
Mixed Layer Density (kg m-3)
Site
E
Subthermocline Layer Depth (m)
F
Subthermocline Layer Temperature (°C)
G
Subthermocline Layer Salinity (PSU)
H
Subthermocline Layer Density (kg m-3)
Site

Figure 2.

Physical seawater properties during the 2015 and 2016 sampling period. A) Mixed layer depths, B) mixed layer temperatures, C) mixed layer salinities, D) mixed layer densities, E) subthermocline layer depths, F) subthermocline layer temperatures, G) subthermocline layer salinities and H) subthermocline layer densities.

The differences in water mass densities between the years were reflected in dissolved nutrient concentrations. Nitrate and silicic acid ($Si[OH]_4$) concentrations within the mixed layer were lower at nearly all sites in 2015 relative to 2016 (Fig. 3a and b). Nitrate concentration in the euphotic zone was significantly lower during the El Niño relative to 2016, with median values of 1.70 µmol L^{-1} and 6.20 µmol L^{-1} respectively (Fig. 3c). Similarly, $Si(OH)_4$ had lower median values in 2015 (1.65 µmol L^{-1}) compared to 2016 (4.99 µmol L^{-1}) (Fig. 3d). Both years had higher NO_3^- concentrations relative to $Si(OH)_4$ concentrations, however the $Si(OH)_4$: NO_3^- slope of the distribution in 2015 was lower (m = 0.40) than in 2016 (m = 0.69), indicating that the concentration of $Si(OH)_4$ relative to NO_3^- was lower during the El Niño (Figure 3e). Overall, physical seawater properties and nutrient concentrations in the GMR show strong temporal trends indicative of oceanographic variation during the 2015/16 El Niño event.

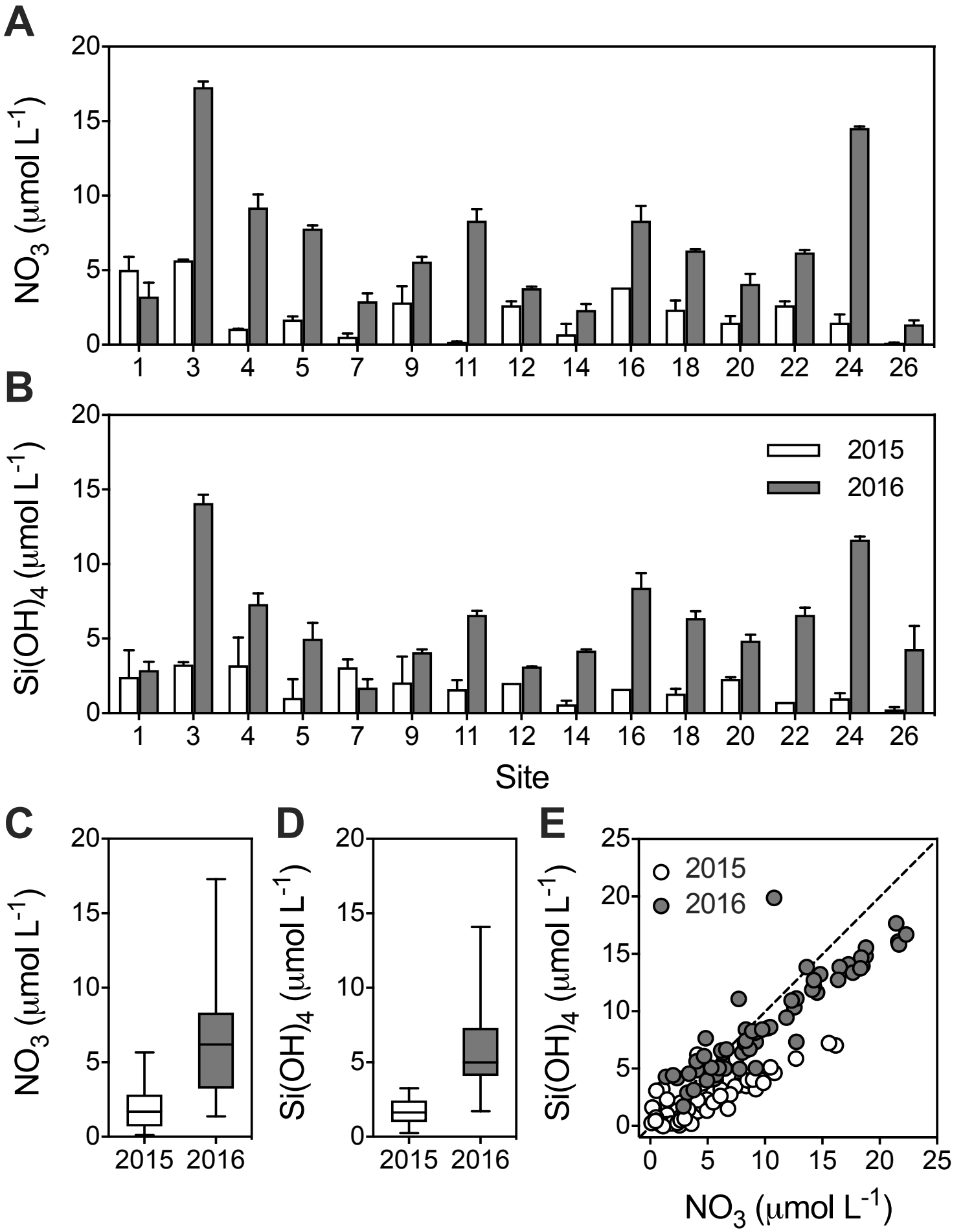
A
B
C
D
E
NO_3 (µmol L^{-1})
$Si(OH)_4$ (µmol L^{-1})
2015
2016
Site
1 3 4 5 7 9 11 12 14 16 18 20 22 24 26
0 5 10 15 20
0 5 10 15 20 25

Figure 3.

Dissolved inorganic nutrients during the 2015 and 2016 sampling period. A) Nitrate (NO_3^-) concentrations. B) silicic acid ($Si[OH]_4$) concentrations. C) interquartile range of NO_3 concentrations at 50% incident irradiance. D) interquartile range of $Si(OH)_4$ concentrations at 50% incident irradiance. E) Scatter plot of NO_3^- verses $Si(OH)_4$ concentrations collected at depths (50%, 30%, 10%, 1% incident irradiance) throughout the euphotic zone. The dashed line represents the 1:1 line. Error bars indicate the standard deviation of the mean (n=2).

Phytoplankton biomass and primary productivity

Chl *a* concentrations were higher in 2016 at most sites with the primary exceptions of sites 14, and 16 (Fig. 4a). The median concentration of the small-size fraction (< 5 μm) was similar between 2015 (0.22 μg L^{-1}) and 2016 (0.23 μg L^{-1}) (Fig. 4b). The large-size fraction (> 5 μm) had a higher median in 2016 (0.2 μg L^{-1}) relative to 2015 (0.13 μg L^{-1}) with a maximum concentration of 1.43 μg L^{-1} in 2016 (Fig. 4c). These are comparable to measurements (89 – 92 ºW, 2 ºS – 1ºN) observed previously during a neutral period, where the average surface Chl *a* was 0.25 μg L^{-1} and the highest concentration (0.53 μg L^{-1}) was recorded west of Isabela island (Torres and Tapia, 2000). In our study, the average small and large size-fractions of Chl *a* did not significantly differ between years, however the large size-fraction showed stronger temporal (p=0.06) and spatial trends, having higher concentrations in 2016 at sites located west of Isabela Island (Fig. 4a and 4d).

Synechococcus flow cytometry cell counts were higher at western sites 3-7 in 2015 than 2016 (Supplementary Figure 3), similar to observations made at the same sites quantified using metagenomics (Gifford *et al.*, 2020). Site four had the greatest difference between the years,

having a concentration of 2.4×10^5 cells mL^{-1} in 2015 and 5.9×10^4 cells mL^{-1} in 2016. The highest *Synechococcus* concentration (2.6×10^5 cells mL^{-1}) was recorded in 2015 at site 14, within the isolated caldera. *Prochlorococcus* was generally more abundant in 2015, particularly in the central and eastern sites, and ranged in concentration from 6.2×10^3 cells mL^{-1} to 1.9×10^5 cells mL^{-1} (Supplementary Figure 3). In 2016 *Prochlorococcus* concentrations were generally lower, ranging from 3.8×10^3 cells mL^{-1} to 1.6×10^4 cells mL^{-1} except at sites five and seven where they were an order of magnitude lower. Picoeukaryotes typically ranged from 10^3-10^4 cells mL^{-1} and had more complex abundance patterns between years than *Synechococcus* and *Prochlorococcus* (Supplementary Figure 3). For example, there were higher concentrations of picoeukaryotes at western sites 4-7 in 2015, while lower concentrations relative to 2016 were recorded at sites 20-26.

Total DIC uptake rates (primary productivity) remained commensurate between years but showed spatial variability, such that sites 3-12 and 18-22 increased during 2016 while other sites decreased (Figure 4e). Insignificant temporal trends in total primary productivity could be attributed to opposite trends in the phytoplankton size-fractions. For instance, median DIC uptake rates in the large size-fraction were 0.46 µmol C L d^{-1} in 2015 to 1.2 µmol C L d^{-1} in 2016, while the small cells decreased from having a median of 1.9 µmol C L d^{-1} in 2015 to 1.44 µmol C L d^{-1} in 2016 (Figure 4g). NO_3^- uptake rates displayed trends similar to Chl *a* and primary productivity such that the large size-fraction differed more between years than the small size-fraction (p=0.07; p=0.87) (Figure 4f and h). The decrease in biomass of the large size-fraction in 2015 coincided with a lower median NO_3^- uptake rate (51.9 nmol N L d^{-1}) in the large size-fraction compared to the small size-fraction (81.4 nmol N L d^{-1}) (Figure 4h). Overall median

366 rates of NO_3^- uptake were greater in both size-fractions during 2016 (129.8, 131.6 nmol N L d^{-1};
367 small and large size-fractions, respectively) (Figure 4h).
368
369
370
371
372
373
374
375
376
377
378
379
380
381
382
383
384
385
386
387
388

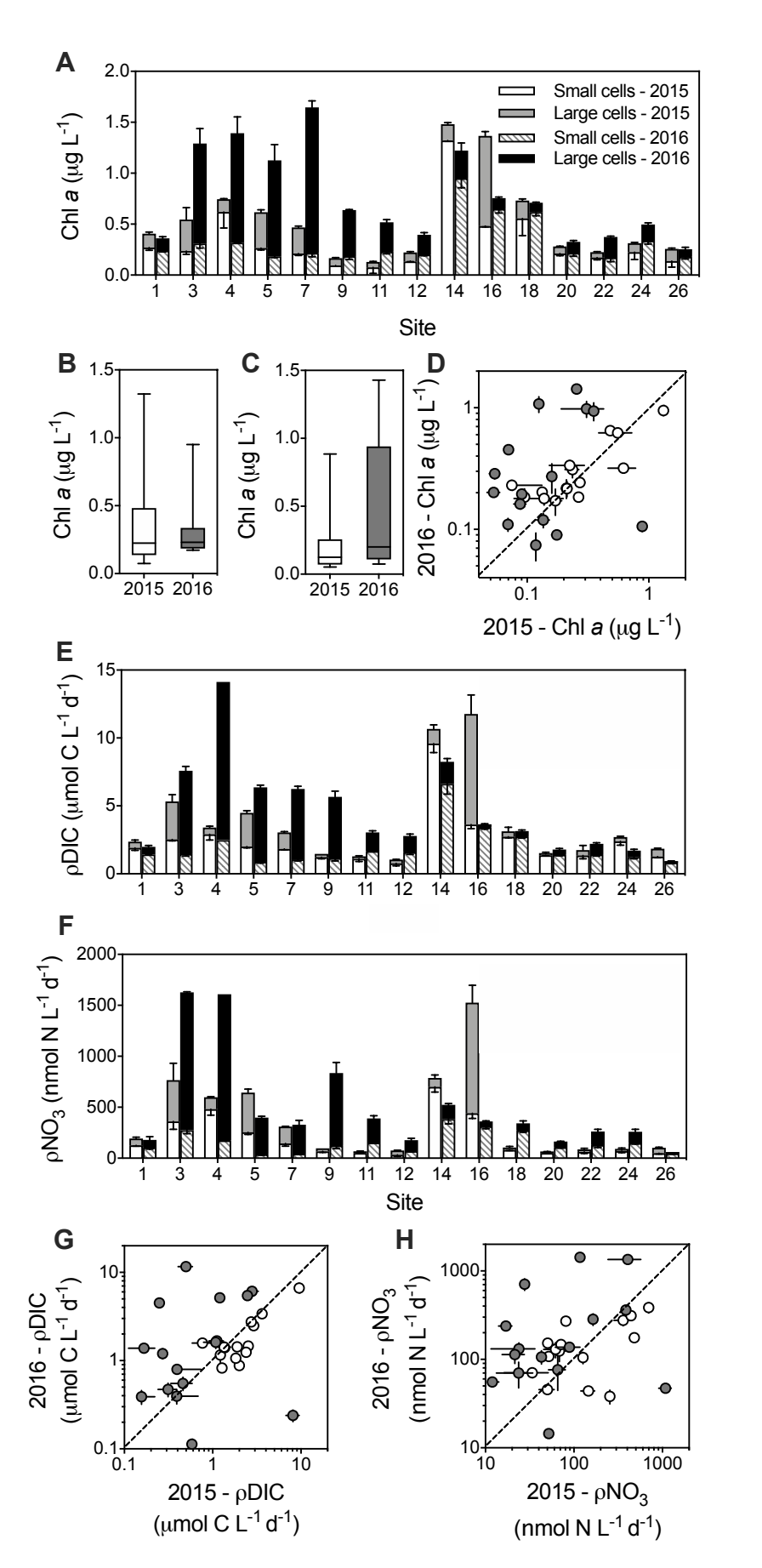
A
Chl a (μg L-1)
Small cells - 2015
Large cells - 2015
Small cells - 2016
Large cells - 2016
Site
B
C
D
2015
2016
2016 - Chl a (μg L-1)
2015 - Chl a (μg L-1)
E
ρDIC (μmol C L-1 d-1)
F
ρNO3 (nmol N L-1 d-1)
Site
G
2016 - ρDIC (μmol C L-1 d-1)
2015 - ρDIC (μmol C L-1 d-1)
H
2016 - ρNO3 (nmol N L-1 d-1)
2015 - ρNO3 (nmol N L-1 d-1)

Figure 4.

Phytoplankton biomass and primary productivity at 50% incident irradiance during the 2015 and 2016 sampling period. A) Size-fractionated chlorophyll *a* (Chl *a*) concentrations. Chl *a* is distinguished between large (> 5 μm) and small (<5 μm) size-fractions. B) interquartile range of Chl *a* concentrations in small cells across all sites and C) interquartile range of Chl *a* concentrations in large cells across all sites. D) Scatter plot of large (grey) and small (white) cell Chl *a* concentrations in 2016 versus 2015. Size-fractionated E) dissolved inorganic carbon uptake rates (i.e. primary productivity; ρDIC) and F) NO_3^- uptake rates (ρNO_3^-). Bar colors are the same as in A. Scatter plot of size-fractionated G) ρDIC and H) ρNO_3^- in 2016 versus 2015. The dashed lines represent the 1:1 line. Symbol colors are the same as in D. Error bars indicate the standard deviation of the mean (n=3). In A, E and F, error bars for the small size-fraction are in the downward direction whereas error bars for the large size-fraction are in the upward direction.

Shifts in protistan community composition

The most proportionally dominant protist groups in the GMR included the dinoflagellates (part of the Alveolata group), chlorophytes, diatoms (part of the Stramenopiles group), Hacrobia, Opisthokont fungi, and Rhizaria (Figure 5a). Collectively, dinoflagellates, chlorophytes, and diatoms dominated the protistan communities and exhibited the most variability between years (Figure 5b-d). Other groups had high spatial variability across sites. For instance, the ciliates and rhizarians were detected at every site in 2015 but lacked detection or genus level identification at over half of the sites in 2016 (Supplemental Fig. 3). Thus, analyses were focused on changes in the three most dominant groups.

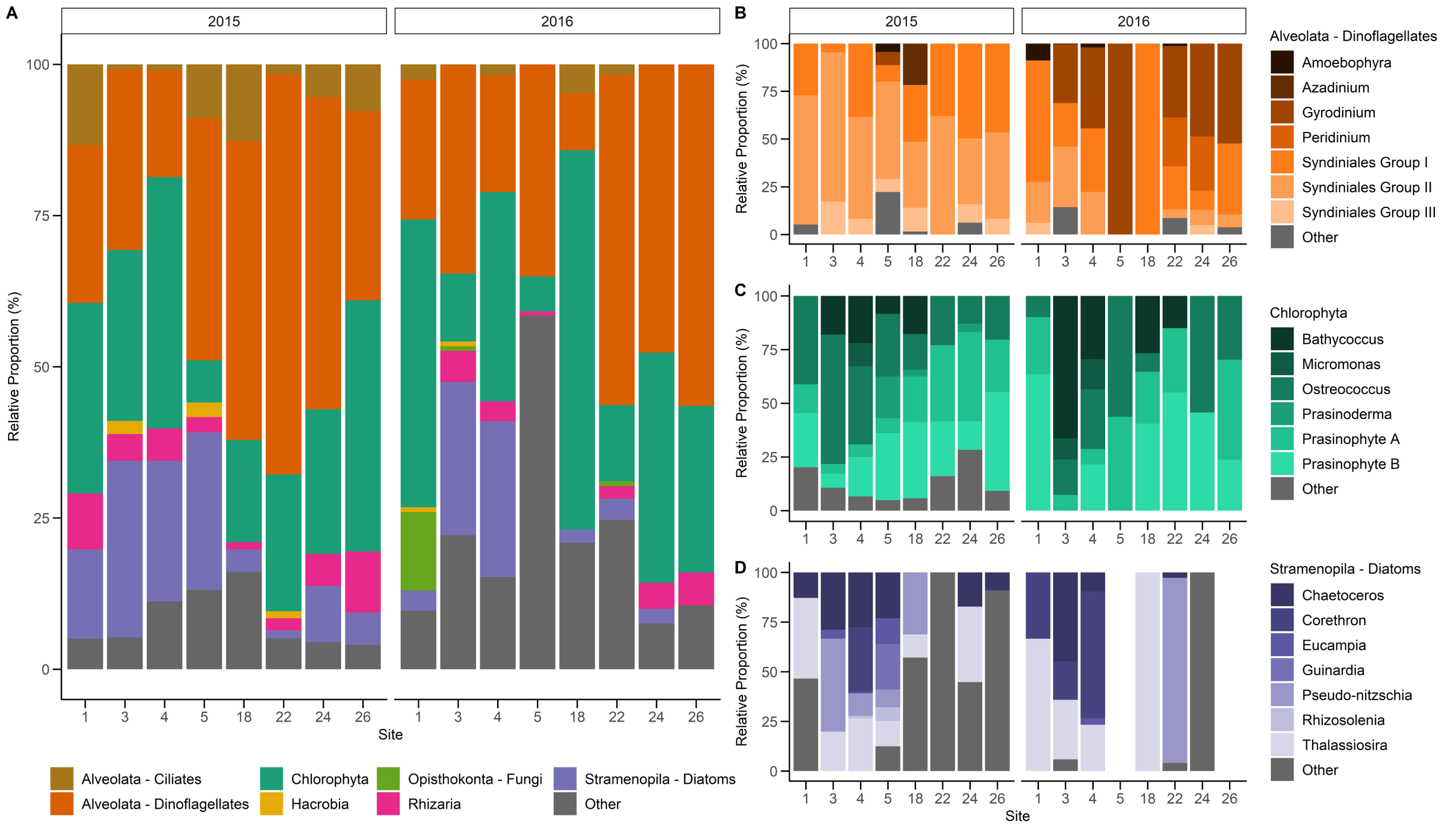
A
2015
2016
Relative Proportion (%)
100
75
50
25
0
1 3 4 5 18 22 24 26
Site
Alveolata - Ciliates
Alveolata - Dinoflagellates
Chlorophyta
Hacrobia
Opisthokonta - Fungi
Rhizaria
Stramenopila - Diatoms
Other
B
Alveolata - Dinoflagellates
Amoebophyra
Azadinium
Gyrodinium
Peridinium
Syndiniales Group I
Syndiniales Group II
Syndiniales Group III
Other
C
Chlorophyta
Bathycoccus
Micromonas
Ostreococcus
Prasinoderma
Prasinophyte A
Prasinophyte B
Other
D
Stramenopila - Diatoms
Chaetoceros
Corethron
Eucampia
Guinardia
Pseudo-nitzschia
Rhizosolenia
Thalassiosira
Other

Figure 5.

Protistan community composition based on 18S rRNA gene amplicons. A) Relative proportions of protists at class level groupings in 2015 and 2016. B) Relative proportions of the Dinoflagellate group, highlighting the top seven most abundant genera. C) Relative proportions of the Chlorophyta group, highlighting the top six most abundant genera. D) Relative proportions of the Diatom group, highlighting the top seven most abundant genera.

The dinoflagellates had a total of 186 OTUs within 21 genera. Dinoflagellate communities were proportionally well represented by seven primary order and genus level groups (Figure 5b). Temporal changes in dinoflagellate proportions between years were more prominent than spatial changes among sites, as indicated by a larger variation along the horizontal axis of the NMDS plot (Figure 6). Changes in dinoflagellate community structure most resembled the collective changes in the density of the subthermocline layer, primary productivity by small cells, and picoeukaryote cell abundance (Spearman's rho = 0.61) (Table 1). Dinoflagellate composition changed the most between years relative to the chlorophytes and diatoms, yet as a broader group they maintained relatively high proportions over the 2015/16 ENSO. This could be due in part to the diverse life strategies that enable dinoflagellates to bloom at various phases of the upwelling cycle (Smayda and Trainer, 2010).

435 **Table 1.**

436 Combinations of variables yielding the 'best matches' of variable (Euclidian) and community
437 (Bray Curtis dissimilarity) matrices using Spearman's rank correlation (rho). The variables are
438 abbreviated such that: lg_updic = dissolved inorganic carbon uptake by the large (>5 µm)
439 phytoplankton size-fraction; pden_dl = potential density of the subthermocline layer; phosphate
440 = phosphate concentration; pico = picoeukaryote flow-cytometry counts; pro = *Prochlorococcus*
441 flow-cytometry counts; sil = silicic acid concentration; sm_updic = dissolved inorganic carbon
442 uptake by the small (<5 µm) phytoplankton size-fraction; sm_upnit = nitrate uptake by the small
443 (<5 µm) phytoplankton size-fraction; syn = *Synechococcus* flow-cytometry counts; temp_ml =
444 temperature of the mixed layer; tot_upnit = total nitrate uptake of both large and small
445 phytoplankton size-fractions. (a) Whole protist community (b) Dinoflagellates (c) Chlorophytes
446 (d) Diatoms

	Environmental & Ecological Variables	**Variables**	**Spearman's Rho**
A. Whole Community			
	tot_upnit, pico, pro, pden_dl	4	0.6239
	tot_upnit, pico, pden_dl	3	0.6216
	tot_upnit, syn, pico, pro, pden_dl	5	0.6189
	tot_upnit, sm_updic, syn, pico, pro, pden_dl	6	0.6179
	sil, tot_upnit, sm_updic, syn, pico, pro, pden_dl	7	0.6099
	sil, sm_upnit, tot_upnit, sm_updic, syn, pico, pro, pden_dl	8	0.6057
	sil, sm_upnit, tot_upnit, sm_updic, syn, pico, pro, pden_dl, temp_ml	9	0.5898

	sil, sm_upnit, tot_upnit, sm_updic, lg_updic, syn, pico, pro, pden_dl, temp_ml	10	0.5676
	syn, pden_dl	2	0.5664
	phosphate, sil, sm_upnit, tot_upnit, sm_updic, lg_updic, syn, pico, pro, pden_dl, temp_ml	11	0.5498
	pden_dl	1	0.3681
B. Dinoflagellates			
	sm_updic, pico, pden_dl	3	0.6063
	sm_updic, pico, pro, pden_dl	4	0.5951
	pico, pden_dl	2	0.566
	sil, sm_updic, syn, pico, pden_dl	5	0.5649
	sil, sm_updic, syn, pico, pro, pden_dl	6	0.5495
	sil, sm_updic, syn, pico, pro, pden_dl, temp_ml	7	0.5183
	phosphate, sil, sm_updic, syn, pico, pro, pden_dl, temp_ml	8	0.4965
	phosphate, sil, sm_updic, lg_updic, syn, pico, pro, pden_dl, temp_ml	9	0.4748
	phosphate, sil, sm_upnit, sm_updic, lg_updic, syn, pico, pro, pden_dl, temp_ml	10	0.4493
	pden_dl	1	0.4222
	phosphate, sil, sm_upnit, tot_upnit, sm_updic, lg_updic, syn, pico, pro, pden_dl, temp_ml	11	0.4143
C. Chlorophytes			
	tot_upnit, pico	2	0.6826
	sm_upnit, syn, pico	3	0.6756

	sm_upnit, syn, pico, pden_dl	4	0.6739
	sm_upnit, tot_upnit, syn, pico, pden_dl	5	0.6733
	sm_upnit, tot_upnit, syn, pico, pro, pden_dl	6	0.6621
	sm_upnit, tot_upnit, lg_updic, syn, pico, pro, pden_dl	7	0.6315
	sm_upnit, tot_upnit, lg_updic, syn, pico, pro, pden_dl, temp_ml	8	0.5947
	pico	1	0.5861
	phosphate, sm_upnit, tot_upnit, lg_updic, syn, pico, pro, pden_dl, temp_ml	9	0.5655
	phosphate, sm_upnit, tot_upnit, sm_updic, lg_updic, syn, pico, pro, pden_dl, temp_ml	10	0.5381
	phosphate, sil, sm_upnit, tot_upnit, sm_updic, lg_updic, syn, pico, pro, pden_dl, temp_ml	11	0.4993
D. Diatoms			
	sm_updic, pro	2	0.3671
	sil, sm_updic, pro	3	0.3585
	sm_updic	1	0.3353
	sil, tot_upnit, sm_updic, pro	4	0.3312
	sil, sm_upnit, tot_upnit, sm_updic, pro	5	0.2969
	sil, sm_upnit, tot_upnit, sm_updic, pro, pden_dl	6	0.2788
	sil, sm_upnit, tot_upnit, sm_updic, pico, pro, pden_dl	7	0.2554
	sil, sm_upnit, tot_upnit, sm_updic, lg_updic, pico, pro, pden_dl	8	0.2341
	sil, sm_upnit, tot_upnit, sm_updic, lg_updic, syn, pico, pro, pden_dl	9	0.2017

	phosphate, sil, sm_upnit, tot_upnit, sm_updic, lg_updic, syn, pico, pro, pden_dl	10	0.1726
	phosphate, sil, sm_upnit, tot_upnit, sm_updic, lg_updic, syn, pico, pro, pden_dl, temp_ml	11	0.1444

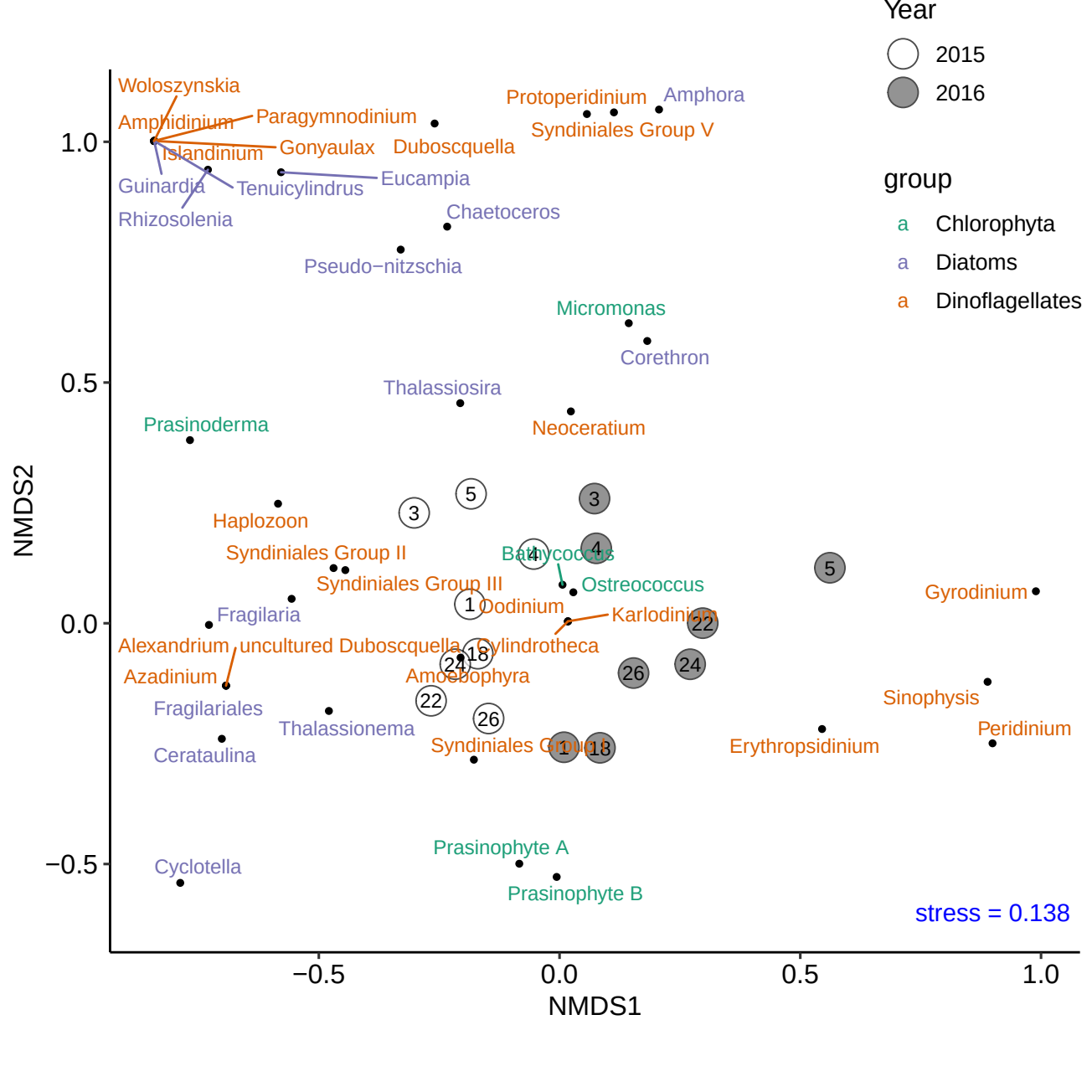
Year
2015
2016
group
a Chlorophyta
a Diatoms
a Dinoflagellates
Woloszynskia
Amphidinium
Paragymnodinium
Gonyaulax
Islandinium
Guinardia
Tenuicylindrus
Eucampia
Rhizosolenia
Protoperidinium
Amphora
Syndiniales Group V
Duboscquella
Chaetoceros
Pseudo−nitzschia
Micromonas
Corethron
Thalassiosira
Prasinoderma
Neoceratium
Haplozoon
Syndiniales Group II
Syndiniales Group III
Bathycoccus
Ostreococcus
Dodinium
Karlodinium
Gyrodinium
Fragilaria
Alexandrium
uncultured Duboscquella
Cylindrotheca
Azadinium
Amoebophyra
Fragilariales
Thalassionema
Sinophysis
Peridinium
Erythropsidinium
Syndiniales Group I
Cerataulina
Prasinophyte A
Prasinophyte B
Cyclotella
stress = 0.138
NMDS1
NMDS2
1.0
0.5
0.0
−0.5
−0.5
0.0
0.5
1.0

Figure 6.

Non-metric Multi-Dimensional Scaling (NMDS) plot showing differences in the whole protistan community composition based on the Bray-Curtis dissimilarity matrix. 2015 sites (white) and 2016 sites (grey) are labelled with site numbers. The loadings for each genera group are plotted as points (black).

Members of the dinoflagellate genus *Gyrodinium* showed the strongest temporal shift, seeming to favor the relatively cooler, higher nutrient conditions present in 2016 such that they were notably represented in the west (sites 3-5) and east (sites 22-26) (Figure 4e). Some *Gyrodinium* species have been found in sediments, and are suspected to form benthic resting cysts which live on internal nutrient reserves for long periods of dormancy until conditions become more favorable for growth (Shang *et al.*, 2019). Along the coasts of Santa Cruz and other small neighboring islands in the central region of the GMR, water column surveys of dinoflagellate communities found that 84% of samples contained benthic epiphytic dinoflagellates (Carnicer *et al.*, 2019), a high percentage given that only ~10% of dinoflagellates associate with a substrate (Hoppenrath *et al.*, no date). The suspension of these epiphytic dinoflagellates in the GMR suggests potential physical mechanisms for benthic resting cyst resuspension. Other cyst forming genera which were detected in our samples include *Alexandrium*, *Gonyaulax*, *Neoceratium*, *Paragymnodinium*, *Peridinium*, *Protoperidinium*, and *Woloszynskia* (Pospelova and Head, 2002; Bravo and Figueroa, 2014; Yokouchi, Onuma and Horiguchi, 2018). *Peridinium* was also detected in 2016 at sites 22 and 24, where it made up a significant proportion of the dinoflagellate community (Figure 5b). Long-term nutrient and temperature stress are the most common causes of resting cyst formation in dinoflagellates

(Bravo and Figueroa, 2014). For example, *Gyrodinium uncatenum*, now renamed *Levanderina fissa*, forms cysts to survive in a dormant resting stage which can last for a duration of months to decades (Anderson, Coats and Tyler, 1985). This and other direct observations of cyst formation in closely related species, suggest that the *Gyrodinium* genus have the ability to survive long-term environmental stress (Bravo and Figueroa, 2014; Shang *et al.*, 2019). Therefore, resting cyst formation may be an important strategy for dinoflagellates to subsist over El Niño events.

Syndiniales are a group of parasitoid dinoflagellates that survive via dinoflagellate or metazoan hosts (Jephcott *et al.*, 2016). Metabarcoding techniques have revealed that these parasites are more prevalent than previously recognized (Guillou *et al.*, 2008), and this too is the case in the GMR. Syndiniales groups I and II were dominant in 2015; both groups were simultaneously detected in 2016 except at sites five and 18. In 2016, site 18 notably had a dinoflagellate community highly dominated by Syndiniales I. Syndiniales III covered a larger spatial extent in 2015 than 2016 but generally followed the same trend as Syndiniales I and II, such that relative proportions were typically less in 2016 (Figure 5b). One caveat of our metabarcoding approach is that it does not distinguish between free-living cells and host associated parasites, which makes the ecological role of Syndiniales difficult to assess. Notwithstanding, higher relative proportions of Syndiniales during the El Niño may be a result of increased infection rates since host cell death precedes the release of Syndiniales spores (Jephcott *et al.*, 2016; Clarke *et al.*, 2019). *Ameobophyra*, a specific Syndiniales genus identified in the GMR (Figure 5b), is estimated to use half of its host's biomass for spores leaving the other half as particulate and dissolved organic matter (Salomon and Stolte, 2010; Jephcott *et al.*, 2016). While Syndiniales can exploit photosynthetic hosts, Syndiniales I have been found to correlate positively with Chl *a*, perhaps implying its association with high host biomass or productive

513 regions (Clarke *et al.*, 2019). Despite the high detection of Syndiniales, particularly during the El
514 Niño, their effect on primary productivity and food web dynamics remains unclear.

515 The chlorophyta or green algae had a total of 163 identified OTUs within six genera. The
516 six genera are displayed with an 'other' group which consists of chlorophytes that could not be
517 identified to the genus level (Figure 5c). The most common genera was *Bathycoccus*, the
518 subclades A and B from clade VII of the prasinophytes (Lopes Dos Santos *et al.*, 2017), which
519 we refer to as Prasinophyte A and Prasinophyte B, and *Ostreococcus*. Prasinophyte A and B
520 made up a large relative proportion at many of the sites (Figure 5c), consistent with other studies
521 within the EEP region (Collado-Fabbri, Vaulot and Ulloa, 2011; de Vargas *et al.*, 2015).

522 Spatial variation in chlorophyte communities was more apparent than shifts associated
523 between years. Prasinophyte A, Prasinophyte B, and *Ostreococcus* were detected at all sites in
524 2015. Similarly in 2016, these groups were detected at all sites except at sites five, 22, and 24
525 which respectively lacked detection of either Prasinophyte B, *Ostreococcus*, or Prasinophyte A.
526 Regardless of year, proportions of prasinophytes were generally highest in the east and slightly
527 decreased westward (Figure 5c). *Ostreococcus* are cosmopolitan in protistan communities of
528 the Peruvian coastal upwelling, and thus thrive under upwelling conditions, which could explain
529 a higher detection at sites associated with the EUC (Collado-Fabbri, Vaulot and Ulloa, 2011; Rii
530 *et al.*, 2016). Moreover, total NO_3^- uptake rates and picoeukaryote cell abundance (via flow
531 cytometry) best explained changes in chlorophyte communities (Spearman's rho = 0.6826)
532 (Table 1); the latter being expected given that many chlorophytes are small enough to be
533 enumerated as picoeukaryotes. Chlorophyte communities showed the most spatial changes
534 relative to the dinoflagellates and diatoms, such that genera spread along the vertical axis of the
535 NMDS plot (Figure 6).

536 The diatoms consisted of 78 identified OTUs within 15 genera. Diatom communities
537 were well represented with seven genera and an 'other' group that mainly comprised of those
538 which were unidentifiable to the genus level (Figure 5d). Diatoms were not detected through 18S
539 sequencing at sites five or 26 in 2016 but may have been present at low abundances. Patterns of
540 primary productivity by small cells and *Prochlorococcus* cell abundance provided the best
541 prediction of diatom community change (Spearman's rho = 0.3671) (Table 1). Given the patchy
542 spatial extent of diatoms detected, the ability to predict the changes in the diatom community
543 from the oceanographic variables was lower relative to the other groups.
544 Two common diatom genera, *Corethron* and *Pseudo-nitzschia* had slight temporal trends
545 and are hypothesized to be somewhat regulated by the EUC upwelling conditions (Torres and
546 Tapia, 2000; McCulloch, 2011). During 2015, *Pseudo-nitzschia* was present at the western sites
547 (sites 3-5) and site 18. Similarly, during the 2006/07 El Niño, *Pseudo-nitzschia* was a dominant
548 phytoplankton species north and west of Isabela Island (McCulloch, 2011). *Pseudo-nitzschia* was
549 however still highly detected in 2016 at site 22. In prior neutral periods, this diatom genus has
550 been observed in patchy distributions (Torres and Tapia, 2000; Tapia and Naranjo, 2012).
551 *Corethron* followed opposite trends, such that it represented a higher proportion at sites 1, 3, and
552 4 in the neutral period while in 2015 it was only detected at site 4. Similarly, a 10-fold decrease
553 in *Corethron* was measured during the 2006/07 El Niño relative to its highest abundance during
554 cooler, neutral periods (McCulloch, 2011). *Pseudo-nitzschia* species are detected in the diatom
555 community even in low nutrient conditions, likely due to physiological advantages, while
556 *Corethron* are present in greater proportions at sites 1-4 in 2016, likely benefitting from the
557 nutrient-rich neutral period. Two other ubiquitous diatom genera, *Chaetoceros* and
558 *Thalassiosira,* were omnipresent in the GMR and have been previously identified during various

559 seasons and stages of ENSO (Torres and Tapia, 1998; McCulloch, 2011; Tapia and Naranjo,
560 2012; Naranjo and Tapia, 2015). *Chaetoceros* can form resting spores anticipatory of upwelling
561 relaxation (Pitcher *et al.*, 1991), fair well under horizontal advection (Tilstone *et al.*, 2015), and
562 germinate rapidly (Smayda, 2000), which may explain their higher proportions at western sites in
563 both 2015 and 2016 (Figure 5d).

564 **Deep water mass properties influence protist communities**

565 The protistan community varied most between the El Niño and neutral periods, but also
566 had some spatial patterns, such that western and eastern sites formed groupings (Figure 6). From
567 the BIO-ENV analysis, this variation in protistan community composition is best explained
568 (Spearman's rho = 0.6239) collectively by patterns of total NO_3^- uptake, picoeukaryote and
569 *Prochlorococcus* cell abundances, and the density of subthermocline layer water masses (Table
570 1). Interestingly, *Synechococcus* abundance and density of the subthermocline layer had the
571 highest BIO-ENV model predictability of any two variables combined (rho = 0.5664) (Table 1).
572 Moreover, regressions between select individual variables and community dissimilarities showed
573 that *Synechococcus* had the highest correlation with community change (R^2 = 0.7271), due to its
574 significant correlation with dinoflagellate and chlorophyte community subgroups
575 (Supplementary Table 4). Dinoflagellates, the subgroup of the protistan community which
576 varied the most, also had the strongest correlation with the density of the subthermocline layer
577 (R^2=0.73) (Supplementary Table 4).

578 In the broader EEP, phytoplankton biomass has been linked to changes in deep water
579 mass conditions below the thermocline, such that decreases in Chl *a* biomass due to El Niño
580 events can be detected before SST anomalies (Park, Dunne and Stock, 2018). Thermocline depth
581 has also previously been identified as important for predicting Chl *a* concentrations in the GMR

582 (Palacios, 2002; Sweet *et al.*, 2007). In this study, the lack of strong correlation between the
583 protistan communities with mixed layer properties is likely due to protists, particularly
584 dinoflagellates, responding to deep water mass shifts before they are detected in the mixed layer.
585 The EUC, a deep nutrient-rich current that slows during El Niño, not only upwells on the western
586 side of the Galápagos platform, but flows horizontally around Isabela Island and continues
587 eastward, providing deep water mass sources from the north and south to the archipelago
588 (Jakoboski *et al.*, 2020). The EUC likely influenced the observed spatio-temporal changes in
589 protistan communities over the 2015/16 El Niño. These observations also provide support that
590 protistan communities change in conjunction with cyanobacteria populations, and that the
591 density of the subthermocline layer is a critical environmental indicator of that shift in
592 community composition, both of which are attributes of the broader EEP (Masotti *et al.*, 2010;
593 Park, Dunne and Stock, 2018).
594
595 **Conclusions**
596 Changes in water density profiles coupled with the nutrient regime suggest an observed
597 weakening of the EUC, selecting for different phytoplankton size classes over the 2015/16
598 ENSO. In 2015, waters were less dense and had lower $Si(OH)_4$:NO_3^- ratios relative to the cooler,
599 2016 neutral period. Increased nutrient availability in 2016 likely led to increases in nitrate
600 utilization by large cells such as diatoms and dinoflagellates. Despite appreciably lower primary
601 productivity at western sites in 2015 compared to 2016, overall primary productivity of
602 phytoplankton communities did not significantly differ across the entire archipelago due to local
603 hotspots during El Niño (e.g., sites 14, 16) and small phytoplankton having higher primary

604 productivity in 2015 at many stations, offsetting the higher NO_3^- uptake in both small and large
605 phytoplankton during 2016.

606 Protistan communities varied distinctly in the GMR during the 2015/16 ENSO.
607 Chlorophytes were detected in high abundance in both years, varied spatially, and correlated
608 with NO_3^- uptake, picoeukaryote abundance, and *Synechococcus*. Diatoms had a patchy spatial
609 extent making causes for changes difficult to discern, yet primary productivity by small cells and
610 *Prochlorococcus* abundances were significant correlates. The largest difference between
611 protistan communities however, was in the dinoflagellate group, such that *Syndiniales* were
612 highly detected in 2015 while *Gyrodinium* were dominant in 2016. Dinoflagellates also
613 happened to correlate strongly with primary productivity of small phytoplankton, picoeukaryote
614 abundance and the density of the subthermocline layer.

615 The strongest correlation between the oceanographic variables and the entire protistan
616 community composition over the 2015/16 ENSO was the density of the subthermocline layer – a
617 proxy for shifts in deep water masses. These findings indicate that the water mass sources are an
618 important factor in influencing protistan seed populations in the mixed layer whereas fluctuations
619 in the short-term oceanographic conditions may have a more profound influence on their overall
620 abundance and physiological status. Our observations provide motivation to continue to
621 understand the effects of El Niño events on the microbial food-webs in the Galápagos
622 Archipelago and the surrounding EEP region; specifically, to identify how changes in
623 productivity and protistan community composition, as a function of altered ocean circulation,
624 will influence higher marine trophic levels.

625

626

Supplemental Information

Additional Methods

Phytoplankton biomass

Chl *a*, a proxy for phytoplankton biomass, was collected in triplicate by gravity filtering 400 ml of seawater through Isopore 5 µm polycarbonate filters (47 mm) to obtain the large size-fraction (> 5 µm). The filtrate was then filtered onto a Whatman GF/F filter (25mm) using an in-line vacuum (≤ 100 mmHg) to obtain the small size-fraction (≤ 5 µm). The filters were extracted in 6 ml of 90% acetone and incubated in the dark at -20 ºC for 24 hours. Raw fluorescence values of the Chl *a* extracts were measured on a Turner Designs 10-AU fluorometer according to the methods of Brand et al. (1981). Dissolved inorganic nutrients (nitrate + nitrite, phosphate and silicic acid) were measured by filtering 30 ml of water through a 0.2 µm filter, using acid-washed syringes into a polypropylene Falcon™ tube. Dissolved nutrient concentrations were analyzed using a OI Analytical Flow Solutions IV auto analyzer by Wetland Biogeochemistry Analytical Services at Louisiana State University.

Picophytoplankton counts, specifically *Prochlorococcus*, *Synechococcus*, and picoeukaryote populations were quantified using flow cytometry. Two ml whole seawater samples were collected at each depth and preserved using a 10% preservative cocktail consisting of 40% phosphate-buffered saline solution (PBS), 10% formalin, and 0.5% glutaraldehyde (Marie, Simon and Vaulot, 2005). Following 15 minutes on ice to allow the preservative to permeate membranes, samples were frozen at -20 °C until analysis onshore. *Prochlorococcus*, *Synechococcus*, and photosynthetic picoeukaryotes in seawater samples were enumerated using a BD FACSCalibur Flow Cytometer and populations characterized as previously described (Johnson *et al.*, 2010). Briefly, cells were excited with a 488 nm laser (15 mW Ar) and inelastic

forward (<15°) scatter, inelastic side (90°) scatter (SSC), green (530 ± 30 nm) fluorescence, orange fluorescence (585 ± 42 nm), and red fluorescence (> 670 nm) emissions were measured. Population mean properties (scatter and fluorescence) were normalized to 1.0 or 2.0 µm yellow green polystyrene beads (Polysciences, Warrington, PA).

Particulate nutrient concentrations and biological uptake rates

Particulate nutrients, DIC and NO_3^- uptake rates were sampled to assess water quality and phytoplankton productivity. Triplicate acid-washed polycarbonate bottles (618 ml) were filled with seawater from each of the four light depths and incubated on deck in tanks for 24 hr, beginning between 6:00 - 8:00am to capture photosynthesis and respiration cycles congruently across sites. The tanks were flushed with surface seawater via a flow-through system and covered with screening to mimic the incident irradiance depths at which the water samples were collected. Tracer isotope additions of ≤ 10% of ambient nutrient concentrations were used to measure uptake rates following methods described in Slawyk et al. (1977) (Slawyk, Collos and Auclair, 1977). For isotope additions in the field, ambient nitrate and bicarbonate were assumed to be 5 µM and 1200 µM, respectively. Nitrite concentration was assumed to be < 5% of ambient N, therefore N uptake rates were assumed to be that of nitrate. Nitrate uptake was measured by adding 0.5 µM ^{15}N-labelled NO_3^- to each bottle prior to incubation (Dugdale and Goering, 1967). Dissolved inorganic carbon (DIC) uptake rates were measured by adding 120 µM ^{13}C-labeled HCO_3 to each bottle prior to incubation (Hama *et al.*, 1983). After incubation, the bottle contents were filtered to capture the plankton community at 24 hr of exposure to the trace isotopes. The large size-fraction (> 5 µm) was filtered onto a 5 µm polycarbonate filter (47 mm) and the remaining filtrate was filtered onto a pre-combusted (450 ºC for 5 hours) GF/F (25 mm) to obtain the small size-fraction (≤ 5 µm). The particles trapped on the 5 µm polycarbonate filters were

673 rinsed with particle-free (0.2 µm filtered) seawater onto a separate pre-combusted GF/F. The
674 filters were dried for 24 to 48 hours in a combustion oven at 60 ºC, wrapped in tin foil squares
675 (30x30mm, Elemental Analysis D1067), pelletized, and stored in a desiccator. Filters were sent
676 to the Stable Isotope Facility at University of California Davis for mass spectrometry analysis.
677 Measurements of particulate nitrogen (PN) and particulate carbon (PC) were obtained
678 simultaneously with uptake rates of nitrate and dissolved inorganic carbon (DIC). Dissolved
679 nitrate concentrations, PN, PC and ^{15}N and ^{13}C atom percentages were used to calculate
680 volumetric NO_3^- uptake and DIC uptake rates of the different size fractions as according to
681 Dugdale and Goering (1967) (Dugdale and Goering, 1967). Samples were not acidified to
682 remove particulate inorganic carbon. NO_3^- uptake rates were not corrected for possible losses of
683 ^{15}N in the form of dissolved organic nitrogen (Bronk, Glibert and Ward, 1994); therefore, the
684 reported values are considered conservative estimates or net uptake. Chl *a*, particulate nutrients
685 and nutrient uptake rates, as well as dissolved nutrient concentrations are displayed in
686 Supplementary Table 3.

687 **Sequence library preparation for 18S amplicon sequencing**

688 For protist taxonomic identification and proportions, four liters of seawater from 50%
689 incident irradiance at the 18S sites (Figure 1a) was filtered using an in-line vacuum (< 100
690 mmHg) through 0.45 µm NES membrane filters (Pall, 47 mm). DNA was extracted from filters
691 using the Qiagen DNeasy Plant Mini Kit (Qiagen, Germantown, MD, USA) and manufacturer
692 provided protocol. DNA concentrations were quantified using the Quant-iT dsDNA High-
693 Sensitivity Assay kit (Life Technologies, Carlsbad, CA, USA). Extracts were diluted either 1:10
694 or 1:100 so that the DNA concentrations were between 20-50 ng/µl.
695

The V4 hypervariable region of the 18S rRNA gene (600 bp) was targeted and amplified using a two-step PCR method described in Quigley et al., 2014. The forward linker primer (5'- TCG TCG GCA GCG TC + *A GAT GTG TAT AAG AGA CAG* + NNNN + **CCAGCASCYGCGGTAATTCC** -3'), and the reverse linker primer (5'- GTC TCG TGG GCT CGG + *AGA TGT GTA TAA GAG ACAG* + NNNN + **ACTTTCGTTCTTGAT** -3') were used in the first PCR and barcodes were attached during the second PCR. The underlined nucleotide bases are the linker sequences, the italicized bases are spacer sequences, the N's are degenerative nucleotide bases (which were not used for this study), and the bold bases are the V4-18S eukaryotic target sequences. The reagents used for the first PCR included 15 µl Milli-Q water, 2.4 µl ExTaq buffer, 1 µl of forward linker primer, 1 µl of reverse linker primer, 1 µl of ExTaq dNTPs, and 0.125 µl of ExTaq enzymes (Takara Bio Inc., Katsastu, Japan). Five µl of diluted DNA extract was added to the reaction mixture. Samples were run in a thermocycler at 95 ºC for 5 min, 30 cycles at 95 ºC for 40 s, 59 ºC for 2 min, and 72 ºC for 1 min, followed by a third stage at 72 ºC for 7 min. Products of the reaction were checked on a 1% agarose gel. Products were cleaned using the Qiagen Qiaquick PCR purification kit (Qiagen, Germantown, MD, USA) and manufacturer provided protocol. The reagents used for the second PCR included 9.5 µl Milli-Q water, 3 µl of barcoded forward primer, 3 µl of barcoded reverse primer, 2 µl ExTaq buffer, 0.5 µl of ExTaq dNTPs, and 0.1 µl of ExTaq enzyme. Two µl of PCR product from the first reaction, diluted to 10 ng/µl was added to the reaction mixture. Samples were run in the thermocycler at 95 ºC for 5 min, 4-10 cycles at 95 ºC for 40 s, 59 ºC for 2 min, and 72 ºC for 1 min, followed by a third stage at 72 ºC for 7 min. Samples were checked on a 1% agarose gel every 2 cycles until faint bands were achieved. Products were excised from the gel and cleaned using the Qiagen Gel Extraction kit (Qiagen, Germantown, MD, USA) and manufacturer provided protocol. DNA

719 concentrations of the products were quantified, and samples were pooled each at a concentration
720 of 10 ng/µl. The pool was run in a single large gel lane on a 1% SYBR Green (Invitrogen,
721 Carlsbad, CA, USA) stained gel. The amplicon library was excised from the gel and submitted
722 for sequencing to the University of North Carolina at Chapel Hill High Throughput Sequencing
723 Facility across two lanes of Illumina MiSeq (2×300 base pairs).
724
725
726
727
728
729
730
731
732
733
734
735
736
737
738
739
740
741

A

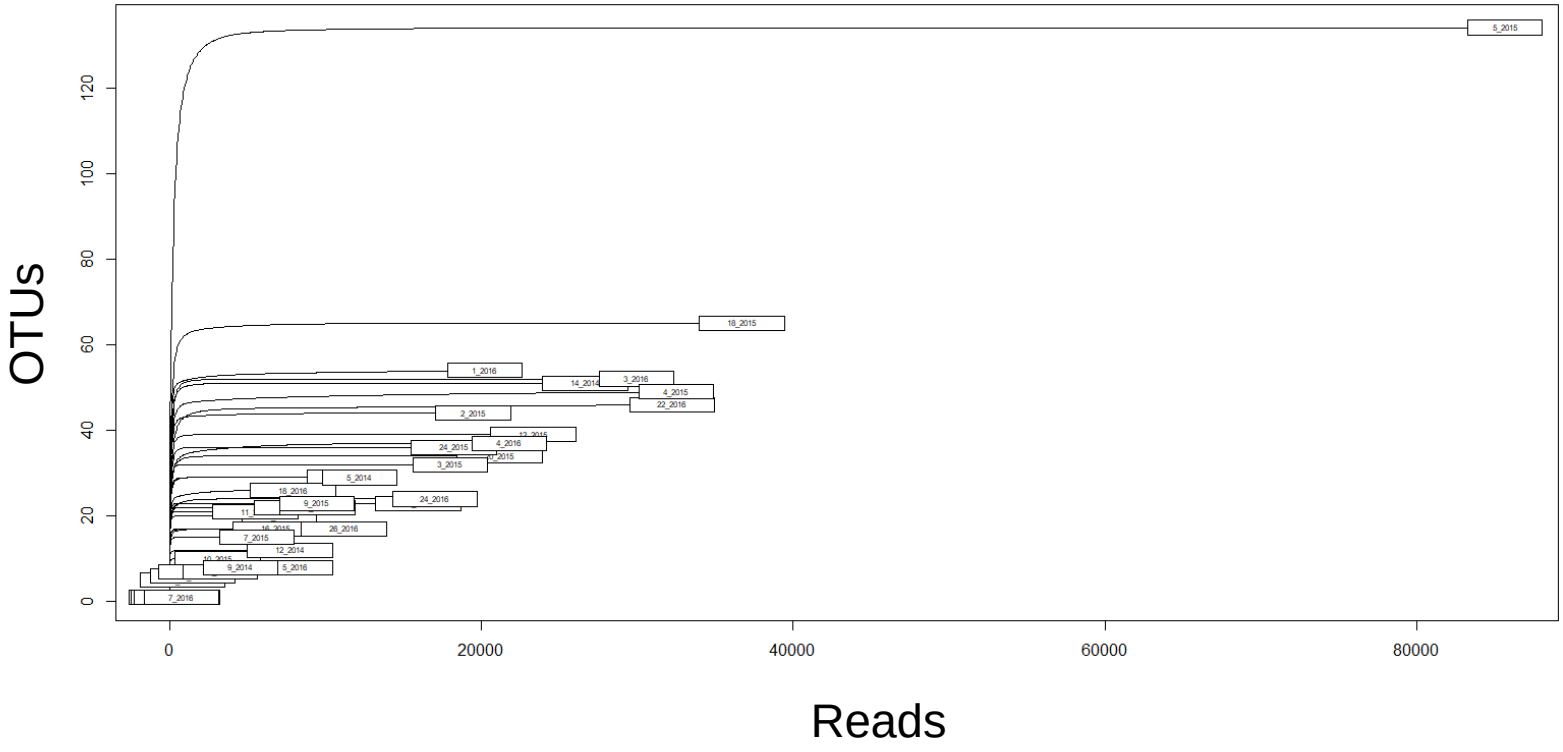

B

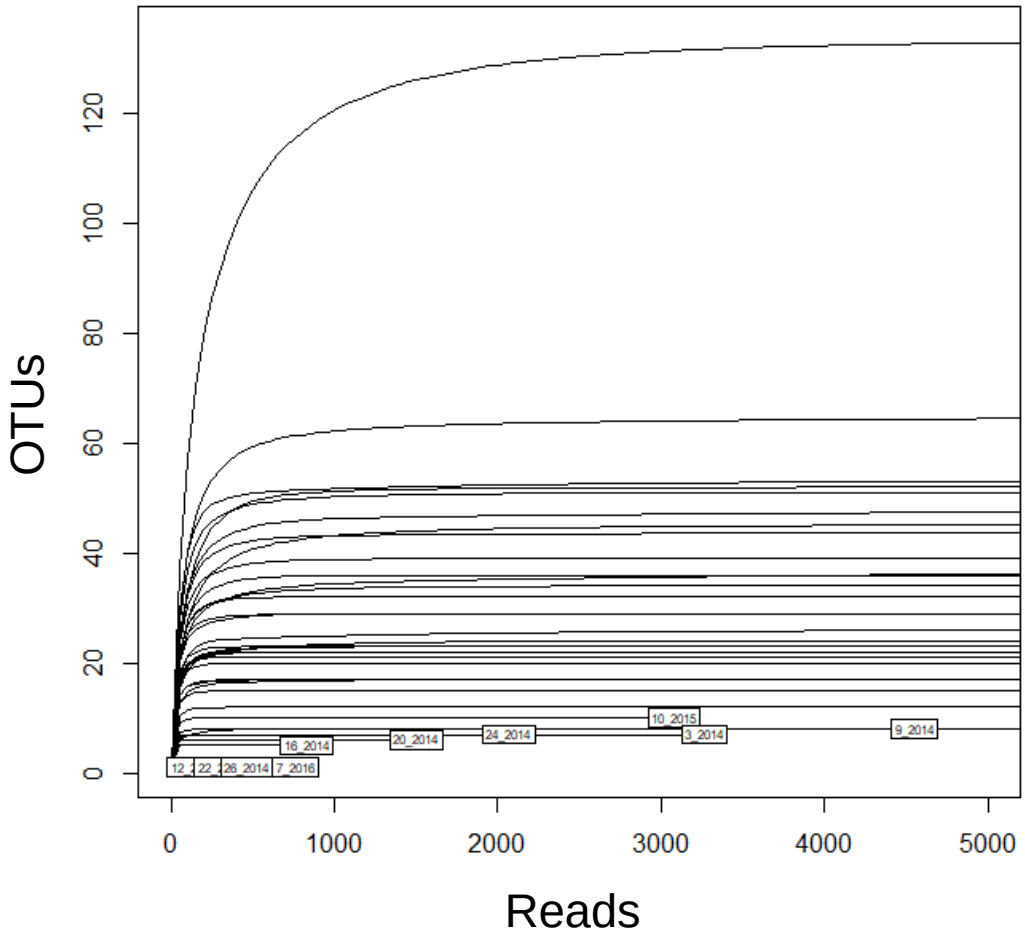

Supplementary Figure 1.

Rarefaction curves (technical replicates have been pooled). A) Rarefaction curves for 39 samples. B) Same as chart A, with x-axis set from 0 to 5000 reads. Samples were rarefied to 2066 reads. Note that OTU values on these plots reflect OTUs before custom taxonomy was assigned.

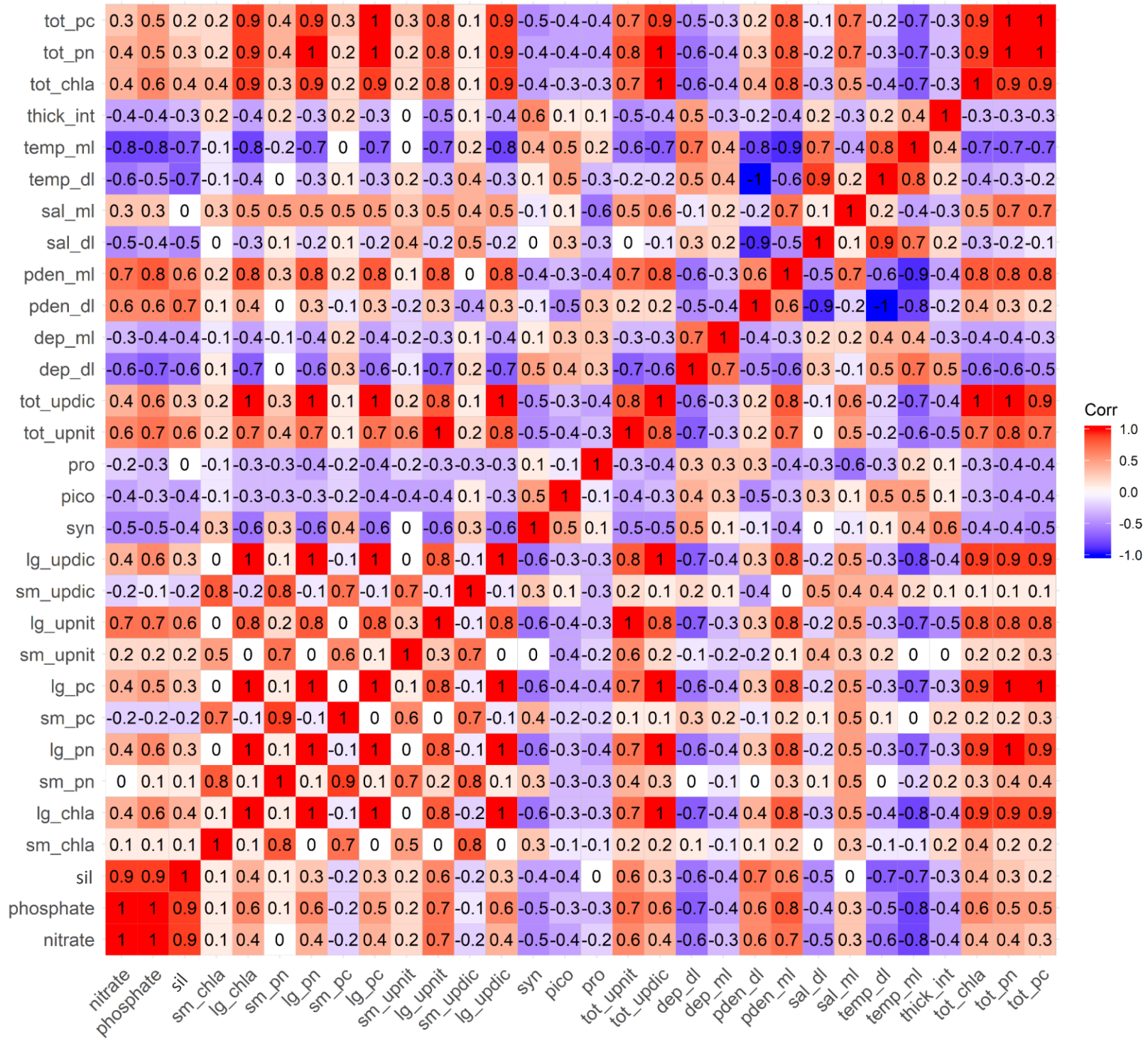

765 **Supplementary Figure 2.**

766 Correlation matrix of variables. Some variables are abbreviated such that: sil = silicic acid
767 concentration; sm_chla = chlorophyll-a concentration (mg/L) of the small (<5 µm)
768 phytoplankton size-fraction; lg_chla = chlorophyll-a concentration (mg/L) of the large (>5 µm)
769 phytoplankton size-fraction; sm_pn = particulate nitrogen (<5 µm); lg_pn = particulate nitrogen
770 (>5 µm); sm_pn = particulate carbon (<5 µm); lg_pn = particulate carbon (>5 µm); sm_upnit =
771 nitrate uptake by the small (<5 µm) phytoplankton size-fraction; lg_upnit = nitrate uptake by the
772 large (>5 µm) phytoplankton size-fraction; sm_updic = dissolved inorganic carbon uptake by the
773 small (<5 µm) phytoplankton size-fraction; lg_updic = dissolved inorganic carbon uptake by the
774 large (>5 µm) phytoplankton size-fraction; syn = *Synechococcus* flow-cytometry counts; pico =
775 picoeukaryote flow-cytometry counts; pro = *Prochlorococcus* flow-cytometry counts; pden_dl =
776 potential density of the subthermocline layer; tot_upnit = total nitrate uptake of both large and
777 small phytoplankton size-fractions; tot_updic = total DIC uptake of both large and small
778 phytoplankton size-fractions; dep_dl = depth of the subthermocline layer; dep_ml = depth of the
779 mixed layer; pden_dl = density of the subthermocline layer; pden_ml = density of the mixed
780 layer; sal_dl = salinity of the subthermocline layer; sal_ml = salinity of the mixed layer; temp_dl
781 = temperature of the subthermocline layer; temp_ml = temperature of the mixed layer; thick_int
782 = distance between the bottom of the mixed layer and top of the subthermocline layer (interfacial
783 layer); tot_chla = total chlorophyll-a concentration (mg/L) of both large and small phytoplankton
784 size-fractions; tot_pc = total particulate carbon of both large and small size-fractions; tot_pn =
785 total particulate nitrogen of both large and small size-fractions.
786
787

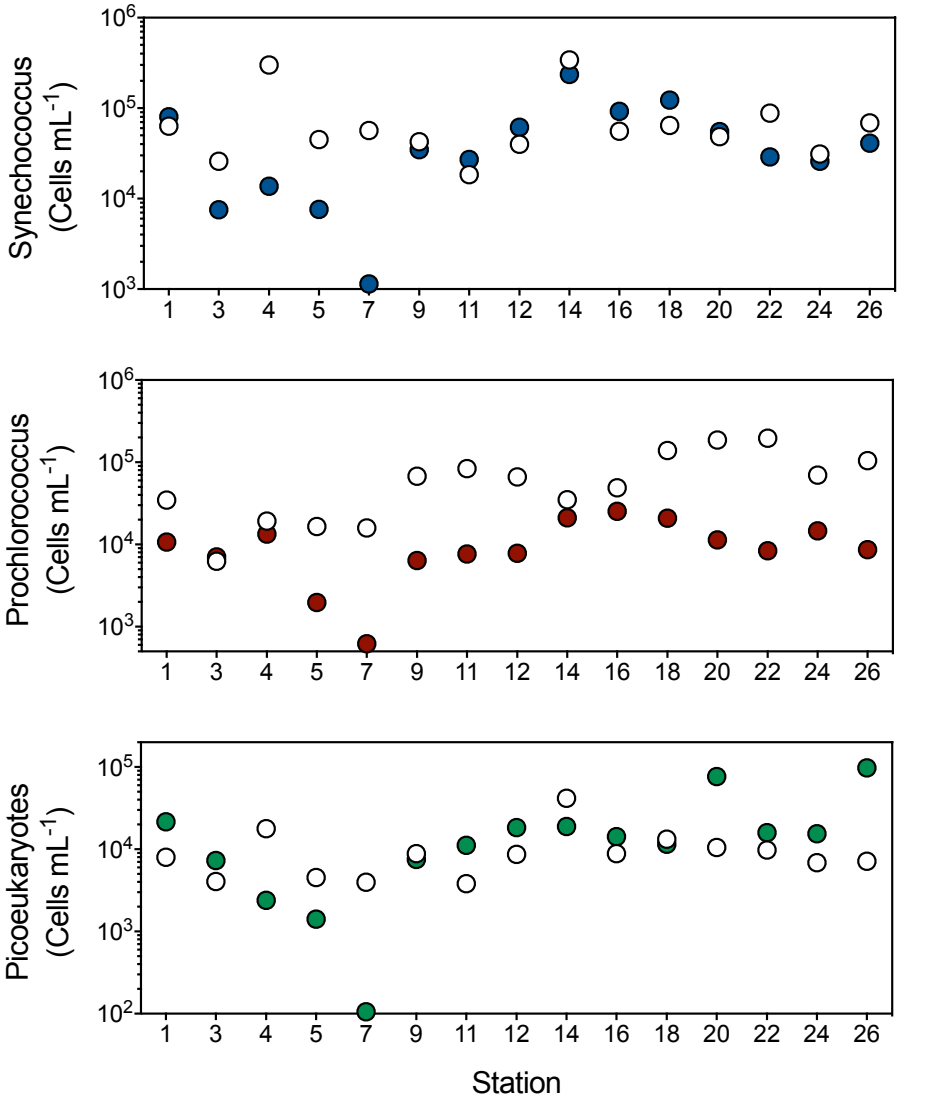
Synechococcus
(Cells mL^{-1})
10^6
10^5
10^4
10^3
1 3 4 5 7 9 11 12 14 16 18 20 22 24 26
Prochlorococcus
(Cells mL^{-1})
10^6
10^5
10^4
10^3
1 3 4 5 7 9 11 12 14 16 18 20 22 24 26
Picoeukaryotes
(Cells mL^{-1})
10^5
10^4
10^3
10^2
1 3 4 5 7 9 11 12 14 16 18 20 22 24 26
Station

Supplementary Figure 3.

Flow cytometry cell counts at sampling sites in 2015 and 2016. White circles indicate cell densities in 2015, while colored circles indicate cell densities in 2016.

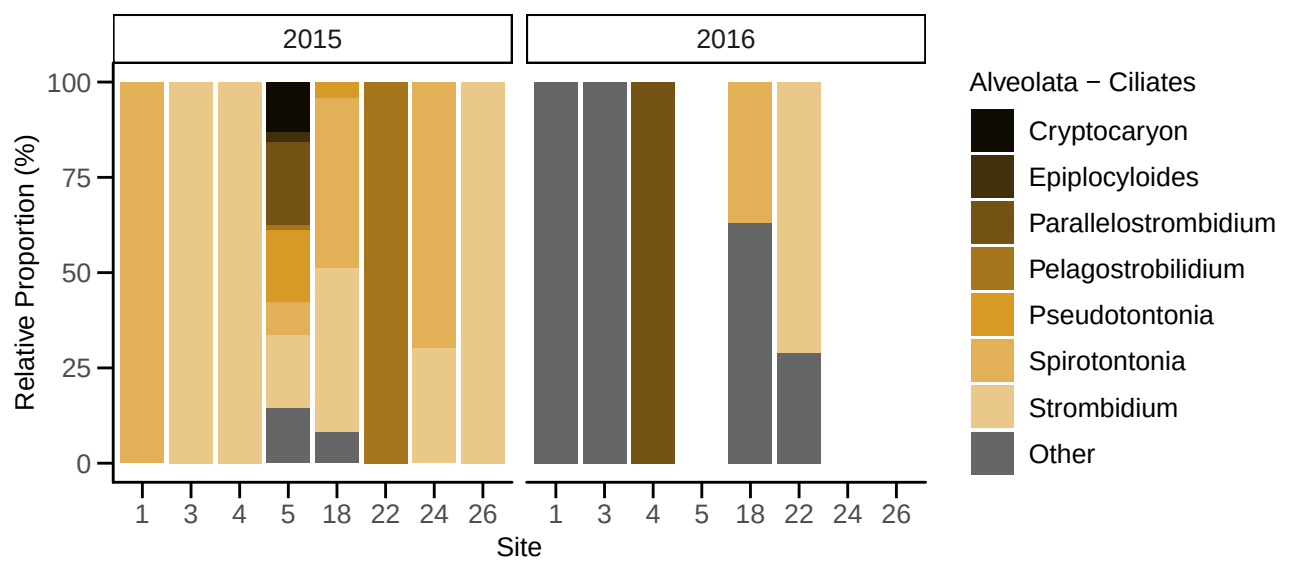
2015
2016
Relative Proportion (%)
100
75
50
25
0
1
3
4
5
18
22
24
26
Site
Alveolata − Ciliates
Cryptocaryon
Epiplocyloides
Parallelostrombidium
Pelagostrobilidium
Pseudotontonia
Spirotontonia
Strombidium
Other

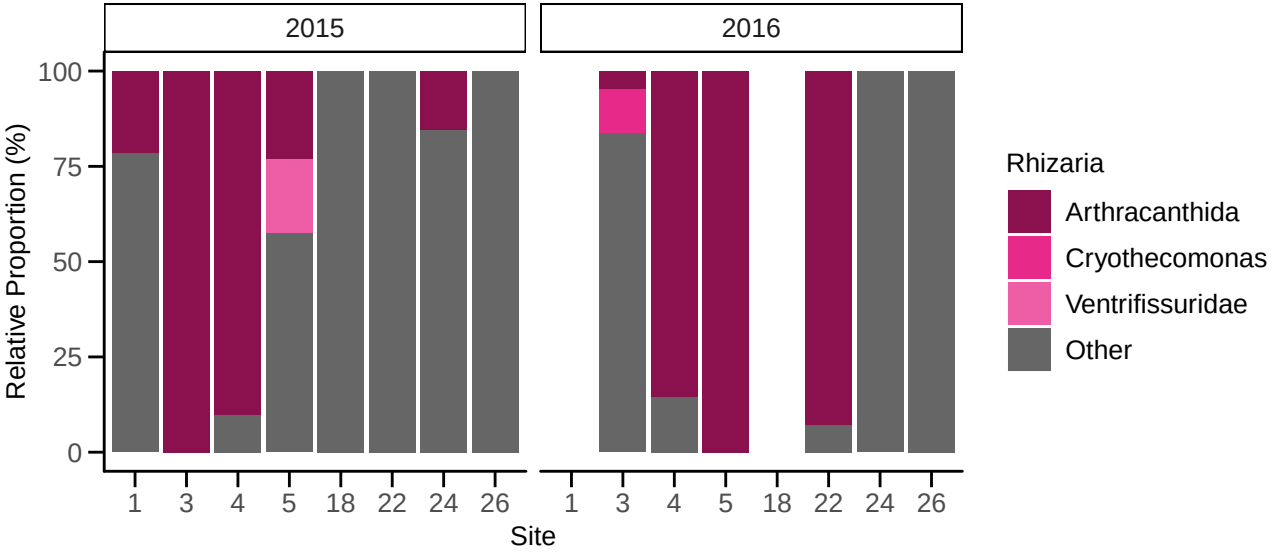
2015
2016
Relative Proportion (%)
100
75
50
25
0
1
3
4
5
18
22
24
26
Site
Rhizaria
Arthracanthida
Cryothecomonas
Ventrifissuridae
Other

Supplementary Figure 4.

Ciliate and Rhizaria 18S rRNA gene community plots. A) Relative proportions of the Ciliate group, highlighting the top seven most abundant genera. B) Relative proportions of the Rhizaria group, highlighting the top three most abundant genera.

Supplementary Table 1.

Table of samples used for 18S rRNA gene analysis of '18S' sites in this study. Samples are derived from bolded samples in Appendix 1, some of which have been pooled from technical replicates to obtain the values below. The final number of reads, or library size, was obtained after blasting the assembled amplicons to the SILVA v. 123 reference database. The number of different OTUs present in each sample before and after rarefication is displayed. OTUs no. values reflect adjustments made to unknown OTUs. If unknown OTUs were present in the same Class they were classified as the same unknown grouping and reflected a single OTU.

Site	Year	Reads						OTUs	
		input	filtered	denoised	merged	non-chimeric	final no. of reads	Raw	After Rarefy
1	2015	60327	27917	27917	13158	10576	7044	14	14
1	2016	191084	152385	152385	130136	28722	20227	15	15
3	2015	176261	52398	52398	24918	19463	17994	17	17
3	2016	86983	71192	71192	56869	33540	29945	26	26
4	2015	149983	120461	120461	94927	43158	32498	19	19
4	2016	130178	76059	76059	65219	26087	21793	19	19
5	2015	845886	761534	761534	589629	145115	85659	56	53
5	2016	21114	17367	17367	14640	11223	8063	8	8
18	2015	188403	100918	100918	59478	45265	36694	26	24
18	2016	62233	45655	45655	37554	8677	7928	10	10
22	2015	93016	53299	53299	33250	23350	15958	12	12
22	2016	187324	171043	171043	116206	46941	32238	22	22
24	2015	100552	66927	66927	42605	26749	18215	20	20
24	2016	78095	71395	71395	52183	22001	17021	12	12
26	2015	51114	34406	34406	20306	17974	11148	12	12
26	2016	43342	37709	37709	27984	19119	11163	10	10

Supplementary Table 2.

Custom taxonomy assigned to the Class taxonomic level (D_2__) originating from the SILVA v. 123 database.

Class	Custom Class
Cryptomonadales	Hacrobia
Kathablepharidae	Hacrobia
Prymnesiophyceae	Hacrobia
Palpitomonas	Hacrobia
Telonema	Hacrobia
Discoba	Excavata
Nucletmycea	Opisthokonts
Picomonadida	Other
Alveolata	Alveolata
Chloroplastida	Chloroplastida
Rhizaria	Rhizaria
Rhodophyceae	Other
Stramenopiles	Stramenopiles
Holozoa	Other

Supplementary Table 3.

Summary statistics for dissolved and particulate nutrients, Chl *a*, primary productivity and nitrate uptake rates. See supplementary Figure 2 for abbreviated variable key.

Variable	mean		median		independent 2-group Mann-Whitney U Test	
	2015	2016	2015	2016	W	p-value
nitrate	2.157467	6.758967	1.6995	6.193	29	0.000264
silicic acid	1.808267	6.081933	1.654	4.985	12	3.51E-06
sm_chla	0.334206	0.349624	0.224223	0.230617	93	0.4306
lg_chla	0.196312	0.422502	0.125355	0.200933	67	0.06128
tot_chla	0.528531	0.772019	0.407707	0.637963	72	0.09753
sm_updic	2.442711	1.962444	1.901882	1.436667	132	0.4363
lg_updic	1.280083	2.673333	0.462093	1.2	78	0.1607
tot_updic	3.707268	4.561556	2.677045	3.146667	89	0.3453
sm_upnit	198.8752	159.2167	81.37914	129.8633	108	0.8702
lg_upnit	169.0535	342.1778	51.91571	131.64	69	0.0742
tot_upnit	367.9203	494.6082	105.1708	329.3867	81	0.2017

year	latitude	longitude	site	NO_3^- (µM)	PO_4^{3-} (µM)	$Si(OH)_4$ (µM)
2015	-1.08327	-91.0913	1	5.0165	0.523	2.4385
2015	-0.46945	-91.6154	3	5.6755	0.796	3.268
2015	-0.44772	-91.3761	4	1.074	0.408	3.1975

2015	-0.28752	-91.6564	5	1.6995	0.4345	1.017
2015	-0.06255	-91.5572	7	0.5475	0.5735	3.0915
2015	0.160683	-91.3097	9	2.853	0.4845	2.0715
2015	0.548283	-90.7919	11	0.193	0.3735	1.618
2015	0.286917	-90.5176	12	2.6645	0.371	1.022
2015	0.306183	-89.9517	14	0.7	0.294	0.613
2015	-0.22822	-90.8716	16	3.851	0.478	1.654
2015	-0.36595	-90.5421	18	2.3585	0.5485	1.328
2015	-0.55573	-90.1461	20	1.48	0.508	2.31
2015	-1.20072	-90.4423	22	2.637	0.5735	2.249
2015	-1.33905	-89.7414	24	1.478	0.445	0.9935
2015	-0.68873	-89.2281	26	0.134	0.383	0.2525
2016	-1.08327	-91.0913	1	3.232	0.524	2.902
2016	-0.46945	-91.6154	3	17.304	1.4265	14.0895
2016	-0.44772	-91.3761	4	9.2245	0.901	7.3305
2016	-0.28752	-91.6564	5	7.7885	0.789	4.985
2016	-0.06255	-91.5572	7	2.908	0.4855	1.7345
2016	0.160683	-91.3097	9	5.603	0.6195	4.098
2016	0.548283	-90.7919	11	8.3315	0.7935	6.599
2016	0.286917	-90.5176	12	3.7985	0.669	3.126
2016	0.306183	-89.9517	14	2.344	0.6065	4.193
2016	-0.22822	-90.8716	16	8.335	0.828	8.4035
2016	-0.36595	-90.5421	18	6.3325	0.7765	6.375
2016	-0.55573	-90.1461	20	4.0875	0.5285	4.876
2016	-1.20072	-90.4423	22	6.193	0.6425	6.594

2016	-1.33905	-89.7414	24	14.535	1.203	11.628
2016	-0.68873	-89.2281	26	1.3675	0.4045	4.295

860

		mean	mean	mean	standard deviation	standard deviation	standard deviation
year	site	sm_pn (nmol/L)	lg_pn (nmol/L)	tot_pn (nmol/L)	sm_pn	lg_pn	tot_pn
2015	1	1392.873	524.3925	1917.266	197.2441	185.0112	193.3588
2015	3	1263.166	1449.514	2712.68	266.6868	245.371	200.0526
2015	4	1709.851	597.4289	2307.28	191.5843	218.3932	26.80889
2015	5	1325.54	1069.004	2394.543	104.2701	31.07704	100.2418
2015	7	906.2676	770.768	1677.036	512.5574	130.8078	389.7119
2015	9	885.3941	650.482	1535.876	73.24488	421.7521	414.527
2015	11	935.1361	340.5332	1275.669	136.0965	43.05484	130.1387
2015	12	695.9137	466.6674	1162.581	376.425	50.11469	425.5941
2015	14	2528.893	470.1441	2999.037	196.9775	125.9723	100.7986
2015	16	1799.034	1804.49	3603.525	339.6629	548.5873	408.6837
2015	18	1271.441	587.7022	1859.143	122.6524	240.593	159.2031
2015	20	976.7436	523.3313	1500.075	519.1229	459.3802	169.1233
2015	22	954.3289	745.4182	1699.747	122.2689	430.922	500.2987
2015	24	927.9323	781.1187	1709.051	553.4452	518.2618	84.22699
2015	26	914.6053	558.8385	1473.444	85.72798	50.27337	98.89218
2016	1	1373.89	783.57	2157.46	33.51172	165.3045	147.6448
2016	3	1374.937	2229.037	3603.973	178.4089	88.74901	146.9314
2016	4	1549.96	3677.58	5227.54	NA	NA	NA

2016	5	1036.717	2463.55	3500.267	97.76806	288.4142	222.2838
2016	7	1860.9	2285.52	4146.42	391.312	223.41	301.7416
2016	9	982.0933	2017.673	2999.767	206.0789	158.0138	68.70205
2016	11	1131.64	848.8333	1226.047	NA	55.91428	663.4499
2016	12	1068.987	949.3067	2018.293	52.88796	306.0843	355.8799
2016	14	2511.533	726.62	3238.153	217.9735	89.13549	142.8141
2016	16	1990.683	311.74	2302.423	98.49966	49.06905	146.9604
2016	18	1794.35	463.16	2257.51	41.18031	166.6094	171.6449
2016	20	1052.63	603.27	1655.9	79.62618	334.6954	402.3871
2016	22	1051.527	589.79	1641.317	28.63359	19.17819	31.44936
2016	24	894.7867	465.64	1360.427	78.99461	63.19213	90.50729
2016	26	859.48	262.4467	1121.927	116.3601	1.403436	117.4547

861

		mean	mean	mean	standard deviation	standard deviation	standard deviation
	site	sm_pc (µmol/L)	lg_pc (µmol/L)	tot_pc (µmol/L)	sm_pc	lg_pc	tot_pc
2015	1	9.012001	2.986874	11.99888	3.130695	0.806295	2.392851
2015	3	7.221374	7.986993	15.20837	1.736978	1.577957	1.762298
2015	4	9.094588	4.202203	13.29679	0.731026	3.01544	2.284415
2015	5	7.280883	7.194916	14.4758	0.70243	0.4825	0.681973
2015	7	5.452462	4.21298	9.665441	3.610194	1.064037	2.569136
2015	9	5.398573	4.390504	9.789077	0.642065	1.530488	1.842264
2015	11	5.435372	1.733863	7.169235	2.25321	0.375027	2.295055
2015	12	3.265884	2.339255	5.60514	1.690878	0.461255	1.942756

2015	14	18.40962	3.196466	21.60609	1.080984	0.941431	0.673006
2015	16	8.67628	11.36877	20.04505	0.630804	3.637747	4.039047
2015	18	7.515143	2.652905	10.16805	0.50914	2.048071	2.279657
2015	20	5.249063	2.658915	7.907978	2.420769	2.532813	0.782465
2015	22	5.715023	3.106268	8.821291	0.715471	2.178608	2.455808
2015	24	4.614055	3.04495	7.659005	2.775506	2.341621	0.481262
2015	26	4.994912	2.326362	7.321275	0.629223	0.459367	0.177925
2016	1	7.948667	4.270667	12.21933	0.276685	0.290676	0.392538
2016	3	6.105	12.52467	18.62967	0.396849	0.488686	0.113271
2016	4	8.564	19.64	28.204	NA	NA	NA
2016	5	5.837333	14.31267	20.15	0.448536	2.132606	1.929112
2016	7	9.226	14.94533	24.17133	1.555803	2.119677	1.038851
2016	9	5.136667	10.45533	15.592	0.499829	0.187961	0.332608
2016	11	6.67	4.841	7.064333	NA	0.732885	3.80346
2016	12	6.918667	4.926667	11.84533	1.163151	0.882565	2.026655
2016	14	14.16233	4.550667	18.713	0.940403	1.000958	1.253807
2016	16	10.67267	1.667667	12.34033	0.387807	0.245875	0.525508
2016	18	9.140667	2.351	11.49167	0.204671	0.293714	0.280293
2016	20	5.861333	3.766333	9.627667	0.397649	2.339338	2.421094
2016	22	5.673333	3.489667	9.163	0.848373	0.502693	0.759947
2016	24	4.616333	2.397	7.013333	0.553079	0.310598	0.264434
2016	26	4.930333	1.583333	6.513667	0.684293	0.137758	0.818881

862

863

		mean	mean	mean	standard deviation	standard deviation	standard deviation
year	site	sm_chla (µg/L)	lg_chla (µg/L)	tot_chla (µg/L)	sm_chla	lg_chla	tot_chla
2015	1	0.271717	0.135991	0.407707	0.027718	0.016219	0.026048
2015	3	0.236097	0.308935	0.545032	0.030888	0.117746	0.101418
2015	4	0.62061	0.125355	0.745965	0.158334	0.00535	0.163629
2015	5	0.264666	0.353442	0.618107	0.018209	0.022634	0.039772
2015	7	0.211	0.256	0.467	0.016371	0.015524	0.025239
2015	9	0.095215	0.070555	0.162551	0.008719	0.00567	0.007266
2015	11	0.074893	0.054252	0.129145	0.057838	0.005434	0.053563
2015	12	0.133411	0.09036	0.226754	0.000736	0.007499	0.006948
2015	14	1.32205	0.159377	1.47686	0.009687	0.014649	0.027125
2015	16	0.48224	0.885477	1.344655	0.009687	0.040417	0.000969
2015	18	0.555307	0.175817	0.731123	0.168015	0.01702	0.152319
2015	20	0.212504	0.069687	0.282192	0.021862	0.002093	0.021853
2015	22	0.17125	0.053247	0.222557	0.021312	0.006255	0.028771
2015	24	0.224223	0.087908	0.312132	0.071481	0.010183	0.079966
2015	26	0.137913	0.118277	0.25619	0.059816	0.009122	0.061939
2016	1	0.24249	0.119601	0.362091	0.014434	0.016421	0.030719
2016	3	0.310533	0.981377	1.29191	0.044315	0.147517	0.189035
2016	4	0.544347	0.91516	1.459507	0.389951	0.298657	0.16115
2016	5	0.184493	0.94119	1.124085	0.013306	0.156935	0.138529
2016	7	0.21783	1.429367	1.647197	0.03858	0.064744	0.101476
2016	9	0.184493	0.45347	0.637963	0.030828	0.007249	0.035205

2016	11	0.230617	0.287243	0.51786	0.021061	0.026577	0.023887
2016	12	0.202303	0.194997	0.3973	0.012729	0.019963	0.032304
2016	14	0.951237	0.27263	1.223867	0.092719	0.07475	0.12273
2016	16	0.649837	0.105901	0.755738	0.040925	0.009882	0.042926
2016	18	0.621067	0.089918	0.710984	0.037577	0.003839	0.033855
2016	20	0.216917	0.109874	0.326791	0.031161	0.013543	0.033058
2016	22	0.17262	0.200933	0.373553	0.041802	0.009623	0.050973
2016	24	0.336107	0.16166	0.497767	0.030888	0.014303	0.031905
2016	26	0.17947	0.074208	0.253678	0.0214	0.019151	0.03997

864

		mean	mean	mean	standard deviation	standard deviation	standard deviation
year	site	sm_updic (µmol/L/day)	lg_updic (µmol/L/day)	tot_updic (µmol/L/day)	sm_updic	lg_updic	tot_updic
2015	1	1.901882	0.462093	2.363976	0.173273	0.126476	0.140799
2015	3	2.531358	2.800502	5.33186	0.10659	0.490954	0.4881
2015	4	2.915005	0.498011	3.413016	0.41805	0.090995	0.327054
2015	5	2.013047	2.476068	4.489115	0.101204	0.158936	0.129727
2015	7	1.83	1.21	2.944496	0.06	0.07	NA
2015	9	1.22093	0.25	1.453445	0.11127	0.01	0.143663
2015	11	1.116283	0.166385	1.282669	0.209437	0.055016	0.196753
2015	12	0.77	0.271957	1.05045	0.1838	0.022101	0.161292
2015	14	9.586615	1.08495	10.67157	0.658968	0.295943	0.408357
2015	16	3.634229	8.14	11.70804	0.302435	1.393	1.787397
2015	18	2.735525	0.392058	3.127583	0.079292	0.293056	0.313838

2015	20	1.37	0.16	1.494396	0.0289	0.0643	0.020774
2015	22	1.353744	0.394033	1.747777	0.246938	0.339962	0.413958
2015	24	2.39	0.313642	2.677045	0.28	0.072618	0.358021
2015	26	1.272052	0.581541	1.853593	0.074504	0.037884	0.106918
2016	1	1.436667	0.553333	1.99	0.045092	0.095044	0.086603
2016	3	1.463333	6.116667	7.58	0.153731	0.332466	0.362905
2016	4	2.49	11.64	14.13	NA	NA	NA
2016	5	0.883333	5.48	6.363333	0.102632	0.167033	0.183394
2016	7	1.066667	5.176667	6.243333	0.106927	0.202073	0.106927
2016	9	1.156667	4.52	5.676667	0.202567	0.420357	0.228108
2016	11	1.67	1.383333	1.94	NA	0.120554	0.86885
2016	12	1.583333	1.2	2.783333	0.150444	0.147309	0.282902
2016	14	6.636667	1.616667	8.253333	0.768722	0.245832	0.645316
2016	16	3.406667	0.24	3.646667	0.106927	0.036056	0.12741
2016	18	2.75	0.396667	3.146667	0.121244	0.075056	0.058595
2016	20	1.406667	0.39	1.796667	0.068069	0.07	0.10504
2016	22	1.42	0.8	2.22	0.117898	0.079373	0.144222
2016	24	1.243333	0.473333	1.716667	0.140119	0.083865	0.105987
2016	26	0.823333	0.113333	0.936667	0.083267	0.015275	0.097125

865

		mean	mean	mean	standard deviation	standard deviation	standard deviation
year	site	sm_upnit (nmol/L/day)	lg_upnit (nmol/L/day)	tot_upnit (nmol/L/day)	sm_upnit	lg_upnit	tot_upnit
2015	1	126.537	65.85543	192.3924	7.746767	14.21564	20.66745

2015	3	360.649	406.502	767.151	76.23357	163.9518	191.7983
2015	4	481.5605	117.6843	599.2448	57.97254	5.541328	52.43121
2015	5	255.933	387.2819	643.2149	22.77127	36.08576	40.91201
2015	7	145.48	164.8	330.6916	25.8	3.07	NA
2015	9	68.6046	27.83	99.93725	11.23629	0.43	13.81445
2015	11	50.73533	16.99245	67.72778	3.744021	2.951693	3.147611
2015	12	33.72984	42.96051	76.69035	17.56143	1.327783	16.71017
2015	14	700.0781	89.2328	789.3109	50.56118	27.78318	31.92963
2015	16	442.6527	1083.56	1501.049	52.54894	171.5795	213.1177
2015	18	81.37914	23.79163	105.1708	5.995178	10.4649	11.39536
2015	20	52.09	11.99	64.87759	4.728152	2.171333	5.795378
2015	22	62.03894	23.87998	85.91892	16.68338	12.30874	22.79962
2015	24	71.54	21.52602	93.39189	18	6.112541	26.60459
2015	26	50.11906	51.91571	102.0348	9.799634	5.009725	14.40122
2016	1	104.79	76.35667	181.1467	15.3993	31.61021	46.85822
2016	3	276.5567	1350.32	1626.877	36.26867	7.136617	43.04111
2016	4	175.58	1433.59	1609.17	NA	NA	NA
2016	5	38.20667	361.2	399.4067	6.825001	11.44844	17.74899
2016	7	44.10667	285.28	329.3867	2.17086	42.98332	42.41468
2016	9	124.5133	710.1967	834.71	30.24171	105.4086	76.82269
2016	11	152.69	238.27	289.1667	NA	25.29497	66.36763
2016	12	70.66	106.9267	177.5867	8.333925	18.41769	26.63488
2016	14	385.41	137.5533	522.9633	49.11438	14.57516	42.55046
2016	16	313.23	47.31333	360.5433	23.72018	5.411851	25.37919
2016	18	272.04	70.41667	342.4567	17.9971	22.97238	18.07291

2016	20	108.0133	55.61333	163.6267	8.421546	3.769421	4.990394
2016	22	129.8633	131.64	261.5033	25.61031	22.77144	47.29522
2016	24	147.0733	113.4967	260.57	6.511777	23.69947	30.02869
2016	26	45.51667	14.49333	60.01	4.736521	1.128952	5.528173

886 **Supplementary Table 4.**

887 Results of the envfit() function. See supplementary Figure 2 for abbreviated variable key.

Variable	Whole Community		Dinoflagellates		Chlorophytes		Diatoms	
	r2	p	r2	p	r2	p	r2	p
sil	0.415	0.030 *	0.3567	0.06	0.0182	0.881	0.2029	0.226
sm_upnit	0.2718	0.123	0.0656	0.651	0.179	0.273	0.249	0.154
lg_upnit	0.6574	0.002 **	0.2137	0.197	0.0575	0.742	0.1827	0.269
sm_updic	0.3484	0.052 .	0.3797	0.037 *	0.197	0.259	0.273	0.117
lg_updic	0.5786	0.006 **	0.1838	0.256	0.1558	0.383	0.1115	0.458
syn	0.7271	0.002 **	0.5775	0.004 **	0.4139	0.019 *	0.009	0.94
tot_upnit	0.6137	0.005 **	0.1051	0.471	0.0155	0.914	0.2468	0.151
pico	0.2389	0.177	0.4262	0.031 *	0.5652	0.011 *	0.0351	0.784
pro	0.6623	0.001 ***	0.3481	0.069 .	0.3555	0.070 .	0.1152	0.474
pden_dl	0.6229	0.002 **	0.7299	0.001 ***	0.1149	0.488	0.0922	0.526
temp_ml	0.4246	0.023 *	0.3341	0.078 .	0.1065	0.48	0.1096	0.467

888

889

890

891

892

893

894

895

896

897

898

899

900

901

Supplementary Table 5.

Table with the values of depth, temperature, salinity, and density of the mixed (ML) and subthermocline (DL) layers obtained from CTD profiles.

		Depth (m)		Potential Density ρ_θ (kg/m^3)		Salinity (PSU)		Temperature (ºC)	
site	Year	DL	ML	DL	ML	DL	ML	DL	ML
1	2015	74.574	41.765	1025.542	1023.962	35.07884	35.00383	17.15188	22.91208
3	2015	54.691	27.844	1025.282	1023.797	35.15576	34.94609	18.45271	23.33218
4	2015	58.667	4.972	1025.361	1022.756	35.15721	34.40935	18.14003	25.45745
5	2015	57.673	26.85	1025.231	1023.143	35.09401	34.58523	18.46886	24.62226
7	2015	44.748	21.878	1025.208	1022.855	35.11656	34.4859	18.62759	25.32338
9	2015	65.627	35.799	1025.274	1023.392	35.00837	34.77897	18.0309	24.28077
11	2015	57.673	10.939	1024.982	1021.94	35.00771	33.71368	19.18724	26.39509
12	2015	58.667	29.833	1024.497	1023.276	34.96258	34.70075	20.89355	24.46823
14	2015	65.627	18.895	1024.493	1022.858	34.79039	34.51659	20.42436	25.38764
16	2015	61.65	51.708	1025.428	1023.722	35.05016	34.91046	17.53284	23.50124
18	2015	70.598	42.759	1025.502	1023.586	35.04397	34.87231	17.20571	23.8639
20	2015	69.604	38.782	1025.196	1023.289	35.0318	34.70571	18.41766	24.43836
22	2015	62.644	20.884	1025.248	1023.283	35.07092	34.6674	18.32925	24.35941
24	2015	48.725	0.995	1025.424	1022.598	35.10714	33.9286	17.72452	24.7792
26	2015	65.627	26.85	1025.393	1022.549	35.11794	34.16701	17.88783	25.53792
1	2016	52.702	8.95	1026.097	1023.58	34.97879	34.21174	14.35497	22.14076
3	2016	25.856	6.961	1026.06	1025.435	34.9931	34.93188	14.57929	17.1086
4	2016	28.839	6.961	1026.049	1025.219	35.00383	34.95251	14.67041	18.06521
5	2016	49.719	1.989	1025.933	1024.737	34.99287	34.699	15.15999	19.21015
7	2016	27.844	13.923	1025.944	1024.843	35.0016	34.86895	15.14143	19.30295
9	2016	51.708	19.889	1025.828	1023.652	34.97766	34.28081	15.5809	22.07181
11	2016	47.731	16.906	1025.993	1024.203	34.9684	34.42807	14.79943	20.46199
12	2016	42.759	7.956	1026.054	1024.023	34.97158	34.33695	14.52727	20.87326
14	2016	26.85	22.872	1024.625	1024.115	34.88242	34.47773	20.18936	20.93247
16	2016	57.673	11.934	1026.055	1024.434	34.967	34.58984	14.5104	20.05481
18	2016	60.656	9.945	1026.007	1024.358	34.97825	34.58253	14.77365	20.32207
20	2016	46.736	38.782	1025.991	1023.382	34.98953	34.00239	14.88439	22.28094
22	2016	31.822	14.917	1025.946	1023.796	35.00014	34.24421	15.12943	21.45189
24	2016	45.742	10.939	1026.012	1023.403	35.01254	33.97096	14.86899	22.11866
26	2016	69.604	32.816	1025.977	1022.714	34.98422	33.64359	14.93502	23.66572

908 **References**

909 Anderson, D. M., Coats, D. W. and Tyler, M. A. (1985) 'Encystment of the dinoflagellate
910 *Gyrodinium uncatenum*: temperature and nutrient effects', *Journal of Phycology*, 21(2),
911 pp.200-206.

912 Barber, R. T., Sanderson, M.P., Lindley, S.T., Chai, F., Newton, J., Trees, C.C., Foley, D.G. and
913 Chavez, F.P. (1996) 'Primary productivity and its regulation in the equatorial Pacific
914 during and following the 1991–1992 El Niño', *Deep Sea Research Part II: Topical*
915 *Studies in Oceanography*, 43(4–6), pp. 933–969.

916 Barber, R. T. and Chavez, F. P. (1991) 'Regulation of primary productivity rate in the equatorial
917 Pacific', *Limnology and Oceanography*, 36(1), pp. 1803–8.

918 Behrenfeld, M. J., Bale, A.J., Kolber, Z.S., Aiken, J. and Falkowski, P.G. (1996) 'Confirmation
919 of iron limitation of phytoplankton photosynthesis in the equatorial Pacific Ocean',
920 *Nature*, *383*(6600), pp. 508–511.

921 Bensted-Smith, R. (1998) 'The special law for Galápagos', *Noticias de Galápagos*, 59(6).

922 Brand, L. E., Guillard, R. R. L. and Murphy, L. S. (1981) 'A method for the rapid and precise
923 determination of acclimated phytoplankton reproduction rates', *Journal of Plankton*
924 *Research*, 3(2), pp. 193–201.

925 Bravo, I. and Figueroa, R. (2014) 'Towards an Ecological Understanding of Dinoflagellate Cyst
926 Functions', *Microorganisms*, 2(1), pp. 11–32.

927 Bronk, D. A., Glibert, P. M. and Ward, B. B. (1994) 'Nitrogen uptake, dissolved organic
928 nitrogen release, and new production', *Science*, 265(5180), pp. 1843–1846.

929 Carnicer, O., De La Fuente, P., Canepa, A., Keith, I., Rebolledo-Monsalve, E., Diogène, J. and
930 Fernández-Tejedor, M. (2019) 'Marine Dinoflagellate Assemblage in the Galápagos

931 Marine Reserve', *Frontiers in Marine Science*, *6*, p.235.

932 Chavez, F. P., Buck, K.R., Service, S.K., Newton, J. and Barber, R.T. (1996) 'Phytoplankton
933 variability in the central and eastern tropical pacific', *Deep-Sea Research Part II: Topical*
934 *Studies in Oceanography*, *43*(4-6), pp.835-870.

935 Chavez, F. P. and Brusca, R. C. (1991) 'The Galápagos Islands and Their Relation to
936 Oceanographic Processes in the Tropical Pacific', In *Galapagos marine*
937 *invertebrates* (pp. 9-33). Springer, Boston, MA.

938 Clarke, K. R. and Ainsworth, M. (1993) 'A method of linking multivariate community structure
939 to environmental variables', *Marine Ecology Progress Series*, 92(3), pp. 205–219.

940 Clarke, L. J. *et al.* (2019) 'A globally distributed Syndiniales parasite dominates the Southern
941 Ocean micro-eukaryote community near the sea-ice edge', *ISME Journal*. Springer US,
942 13(3), pp. 734–737.

943 Collado-Fabbri, S., Vaulot, D. and Ulloa, O. (2011) 'Structure and seasonal dynamics of the
944 eukaryotic picophytoplankton community in a wind-driven coastal upwelling ecosystem',
945 *Limnology and Oceanography*, 56(6), pp. 2334–2346.

946 De Vargas, C., Audic, S., Henry, N., Decelle, J., Mahé, F., Logares, R., Lara, E., Berney, C., Le
947 Bescot, N., Probert, I. and Carmichael, M. (2015) 'Eukaryotic plankton diversity in the
948 sunlit ocean', *Science*, *348*(6237).

949 Dugdale, R. C. and Goering, J. J. (1967) 'Uptake of new and regenerated forms of nitrogen in
950 primary productivity', *Limnology and Oceanography*, 12(2), pp.196-206.

951 Edgar, G. J., Bustamante, R.H., Farina, J.M., Calvopina, M., Martinez, C. and Toral-Granda,
952 M.V. (2004) 'Bias in evaluating the effects of marine protected areas: The importance of
953 baseline data for the Galapagos Marine Reserve', *Environmental Conservation*, pp.212-

218.

Feldman, G. C. (1986) 'Patterns of phytoplankton production around the Galapagos Islands', In *Tidal Mixing and Plankton Dynamics* (pp. 77-106). Springer, New York, NY.

Fiedler, P. C. and Talley, L. D. (2006) 'Hydrography of the eastern tropical Pacific: A review', *Progress in Oceanography*, 69(2–4), pp. 143–180.

Gifford, S. M., Zhao, L., Stemple, B., DeLong, K., Medeiros, P.M., Seim, H. and Marchetti, A. (2020) 'Microbial Niche Diversification in the Galápagos Archipelago and Its Response to El Niño', *Frontiers in Microbiology*, *11*, p.2636.

Guillou, L., , Viprey, M., Chambouvet, A., Welsh, R.M., Kirkham, A.R., Massana, R., Scanlan, D.J. and Worden, A.Z. (2008) 'Widespread occurrence and genetic diversity of marine parasitoids belonging to Syndiniales (Alveolata)', *Environmental microbiology*, *10*(12), pp.3349-3365.

Hama, T., Miyazaki, T., Ogawa, Y., Iwakuma, T., Takahashi, M., Otsuki, A. and Ichimura, S. (1983) 'Measurement of Photosynthetic Production of a Marine Phytoplankton Population Using a Stable 13 C Isotope', *Marine Biology*, 73(1), pp. 31–36.

Hoppenrath, M., Murray, S.A., Chomérat, N. and Horiguchi, T. (2014) Marine benthic dinoflagellates: unveiling their worldwide biodiversity.

Jakoboski, J., Todd, R.E., Owens, W.B., Karnauskas, K.B. and Rudnick, D.L. (2020) 'Bifurcation and upwelling of the equatorial undercurrent west of the Galápagos archipelago', *Journal of Physical Oceanography*, 50(4), pp. 887–905.

Jephcott, T. G., Alves-De-Souza, C., Gleason, F.H., Van Ogtrop, F.F., Sime-Ngando, T., Karpov, S.A. and Guillou, L. (2016) 'Ecological impacts of parasitic chytrids, syndiniales and perkinsids on populations of marine photosynthetic dinoflagellates', *Fungal Ecology*.

977 Elsevier, 19, pp. 47–58.

978 Johnson, Z., I. Shyam, R., Ritchie, A.E., Mioni, C., Lance, V.P., Murray, J.W. and Zinser, E.R.
979 (2010) 'The effect of iron-and light-limitation on phytoplankton communities of deep
980 chlorophyll maxima of the western Pacific Ocean', *Journal of Marine Research*, 68(2),
981 pp. 283–308.

982 Kessler, W. S. (2006) 'The circulation of the eastern tropical Pacific: A review', *Progress in*
983 *Oceanography*, 69(2-4), pp.181-217.

984 Kislik, E., Mantilla, G., Torres, G. and Borbor-Córdova, M. (2017) 'Biological Hotspots in the
985 Galápagos Islands: Exploring Seasonal Trends of Ocean Climate Drivers to Monitor
986 Algal Blooms', *International Scholarly and Scientific Research & Innovation*, 11(12), pp.
987 824–834.

988 Lindley, S. T. and Barber, R. T. (1998) 'Phytoplankton response to natural and experimental iron
989 addition', *Deep-Sea Research Part II: Topical Studies in Oceanography*, 45(6), pp.
990 1135–1150.

991 Liu, Y., Xie, L., Morrison, J.M., Kamykowski, D. and Sweet, W.V. (2014) 'Ocean Circulation
992 and Water Mass Characteristics around the Galápagos Archipelago Simulated by a
993 Multiscale Nested Ocean Circulation Model', *International Journal of Oceanography*,
994 pp. 1–16.

995 Lopes Dos Santos, A., Pollina, T., Gourvil, P., Corre, E., Marie, D., Garrido, J.L., Rodríguez, F.,
996 Noël, M.H., Vaulot, D. and Eikrem, W. (2017) 'Chloropicophyceae, a new class of
997 picophytoplanktonic prasinophytes', *Scientific Reports*, 7(1), pp. 1–20.

998 Marchetti, A., Varela, D.E., Lance, V.P., Lance, V.P., Palmucci, M., Giordano, M. and Virginia
999 Armbrust, E. (2010) 'Iron and silicic acid effects on phytoplankton productivity,

diversity, and chemical composition in the central equatorial Pacific Ocean', *Limnology and Oceanography*, 55(1), pp. 11–29.

Marie, D., Simon, N. and Vaulot, D. (2005) 'Phytoplankton cell counting by flow cytometry', *Algal culturing techniques*. Elsevier Academic Press Burlington, MA, 1, pp. 253–267.

Masotti, I., Moulin, C., Alvain, S., Bopp, L., Tagliabue, A. and Antoine, D. (2011) 'Large-scale shifts in phytoplankton groups in the Equatorial Pacific during ENSO cycles', *Biogeosciences*, *8*(3), pp.539-550.

Maxwell, D.C., (1975) 'Marine primary productivity of the Galapagos archipelago', (Doctoral dissertation, The Ohio State University).

McCulloch, A. (2011) 'A Spatio-Temporal Context for the Phytoplankton Community Patterns of the Galapagos Archipelago and the Northwest Florida Shelf', (Doctoral dissertation, North Carolina State University).

Moore, L. R., Post, A.F., Rocap, G. and Chisholm, S.W. (2002) 'Utilization of different nitrogen sources by the marine cyanobacteria Prochlorococcus and Synechococcus', *Limnology and Oceanography*, 47(4), pp. 989–996.

Naranjo, C. and Tapia, M. E. (2015) 'Plancton en el canal bolívar de la isla isabela (caleta tagus), islas galápagos durante marzo de 2009.', *Acta Oceanográfica del Pacífico*, 20(1).

Palacios, D. M. (2002) 'Factors influencing the island-mass effect of the Galápagos Archipelago', *Geophysical Research Letters*, 29(23), pp.49-1.

Palacios, D. M. (2004) 'Seasonal patterns of sea-surface temperature and ocean color around the Galápagos: Regional and local influences', *Deep-Sea Research Part II: Topical Studies in Oceanography*, *51*(1-3), pp.43-57.

Park, J., Dunne, J. P. and Stock, C. A. (2018) 'Ocean chlorophyll as a precursor of ENSO: An

earth system modeling study', *Geophysical Research Letters*, 45(4), pp.1939-1947.

Pennington, J. T., Mahoney, K.L., Kuwahara, V.S., Kolber, D.D., Calienes, R. and Chavez, F.P. (2006) 'Primary production in the eastern tropical Pacific: A review', *Progress in Oceanography*, *69*(2-4), pp.285-317.

Pitcher, G. C., Walker, D.R., Mitchell-Innes, B.A. and Moloney, C.L. (1991) 'Short-term variability during an anchor station study in the southern Benguela upwelling system: Phytoplankton dynamics', *Progress in Oceanography*. Pergamon, 28(1–2), pp. 39–64.

Pospelova, V. and Head, M. J. (2002) 'Islandinium brevispinosum sp. nov. (Dinoflagellata), a new organic-walled dinoflagellate cyst from modern estuarine sediments of New England (USA)', *Journal of Phycology*, 38(3), pp. 593–601.

Quigley, K. M., Davies, S.W., Kenkel, C.D., Willis, B.L., Matz, M.V. and Bay, L.K. (2014) 'Deep-Sequencing Method for Quantifying Background Abundances of Symbiodinium Types: Exploring the Rare Symbiodinium Biosphere in Reef-Building Corals', *PLoS ONE*, 9(4), p. e94297.

Rafter, P. A., Sigman, D. M. and Mackey, K. R. M. (2017) 'Recycled iron fuels new production in the eastern equatorial Pacific Ocean', *Nature Communications*. Springer US, 8(1).

Rii, Y. M., Duhamel, S., Bidigare, R.R., Karl, D.M., Repeta, D.J. and Church, M.J. (2016) 'Diversity and productivity of photosynthetic picoeukaryotes in biogeochemically distinct regions of the South East Pacific Ocean', *Limnology and Oceanography*, 61(3), pp. 806–824.

Sakamoto, C. M., Millero, F.J., Yao, W., Friederich, G.E. and Chavez, F.P. (1998) 'Surface seawater distributions of inorganic carbon and nutrients around the Galapagos Islands: Results from the PlumEx experiment using automated chemical mapping', *Deep-Sea*

Research Part II: Topical Studies in Oceanography, 45(6), pp. 1055–1071.

Salomon, P. and Stolte, W. (2010) 'Predicting the population dynamics in Amoebophrya parasitoids and their dinoflagellate hosts using a mathematical model', *Marine Ecology Progress Series*, 419, pp. 1–10.

Santoso, A., Mcphaden, M. J. and Cai, W. (2017) 'The Defining Characteristics of ENSO Extremes and the Strong 2015/2016 El Niño', *Reviews of Geophysics*, 55(4), pp. 1079–1129.

Sartory, D. P. and Grobbelaar, J. U. (1984) 'Extraction of chlorophyll a from freshwater phytoplankton for spectrophotometric analysis', *Hydrobiologia*. Springer, 114(3), pp. 177–187.

Schaeffer, B. A., B.A., Morrison, J.M., Kamykowski, D., Feldman, G.C., Xie, L., Liu, Y., Sweet, W., McCulloch, A. and Banks, S. (2008) 'Phytoplankton biomass distribution and identification of productive habitats within the Galapagos Marine Reserve by MODIS, a surface acquisition system, and in-situ measurements', *Remote Sensing of Environment*. Elsevier, 112(6), pp. 3044–3054.

Shang, L., Hu, Z., Deng, Y., Liu, Y., Zhai, X., Chai, Z., Liu, X., Zhan, Z., Dobbs, F.C. and Tang, Y.Z. (2019) 'Metagenomic sequencing identifies highly diverse assemblages of dinoflagellate cysts in sediments from ships' ballast tanks', *Microorganisms*, 7(8), p.250.

Slawyk, G., Collos, Y. and Auclair, J. (1977) 'The use of the 13C and 15N isotopes for the simultaneous measurement of carbon and nitrogen turnover rates in marine phytoplankton', *Limnology and Oceanography*, 22(5), pp. 925–932.

Smayda, T. J. (2000) 'Ecological features of harmful algal blooms in coastal upwelling ecosystems', *African Journal of Marine Science*, *22*.

1069 Smayda, T. J. and Trainer, V. L. (2010) 'Dinoflagellate blooms in upwelling systems: Seeding,
1070 variability, and contrasts with diatom bloom behaviour'. *Progress in*
1071 *Oceanography*, *85*(1-2), pp.92-107.
1072 Sweet, W. V., Morrison, J.M., Kamykowski, D., Schaeffer, B.A., Banks, S. and McCulloch, A.
1073 (2007) 'Water mass seasonal variability in the Galápagos Archipelago', *Deep-Sea*
1074 *Research Part I: Oceanographic Research Papers*, *54*(12), pp.2023-2035.
1075 Tapia, M. and Naranjo, C. (2012) 'Aspectos oceanográficos del plancton y su relación con el
1076 frente ecuatorial, durante septiembre del 2011', *Acta Oceanográfica del Pacífico*,
1077 17(5934), pp.67-91.
1078 Tilstone, G. H., Taylor, B.H., Blondeau-Patissier, D., Powell, T., Groom, S.B., Rees, A.P. and
1079 Lucas, M.I. (2015) 'Comparison of new and primary production models using SeaWiFS
1080 data in contrasting hydrographic zones of the northern North Atlantic', *Remote Sensing of*
1081 *Environment*, 156, pp.473-489.
1082 Torres, G. (1998) 'Variabilidad anual del fitoplancton marino en áreas costeras de La Libertad y
1083 Manta (Ecuador), su inter-relación con eventos El Niño', *Acta Oceanográfica del*
1084 *Pacífico, INOCAR*, *9*(1), pp.115-128.
1085 Torres, G. and Tapia, M.E., 1998. Distribución del primer nivel trófico (fitoplancton) en el
1086 Pacífico ecuatoriano, período 1996-1997 (pre-El Niño). *Acta Oceanográfica del*
1087 *Pacífico*, *9*(1).
1088 Torres, G. and Tapia, M. (2000) 'Distribución del fitoplancton y su comportamiento en el
1089 afloramiento en las Islas Galápagos, *Acta Oceanográfica del Pacífico*, 10(1), pp.137-150.
1090 Torres, G. and Tapia, M. (2002) 'Distribución del fitoplancton en la región costera del mar
1091 ecuatoriano, durante diciembre 2000', *Acta Oceanográfica del Pacífico*, 11(1).

Yokouchi, K., Onuma, R. and Horiguchi, T. (2018) ‘Ultrastructure and phylogeny of a new species of mixotrophic dinoflagellate, Paragymnodinium stigmaticum sp. nov. (Gymnodiniales, Dinophyceae)’, *Phycologia*, 57(5), pp. 539–554. doi: 10.2216/17-140.1.

Acknowledgments

We thank scientists and staff from the Galápagos Science Center (GSC), Universidad San Francisco de Quito (USFQ), and Galápagos National Park (GNP) for their logistical support during the cruises. We are grateful to Steve Walsh (UNC), Carlos Mena (USFQ) and Phil Page (UNC) for their efforts in coordinating the Galápagos Marine Expeditions. Others include Juan Pablo Muñoz (GSC), Leandro Vaca (GSC), Eduardo Espinoza (GNP), Jennifer Suarez (GNP) and the crew of the M/V Sierra Negra. We thank Sara Haines for assistance with processing and visualizing physical and chemical observations. We are grateful to Kimberly DeLong, Sharla Sugierski and Wilton Burns for assistance with sample analyses. Natalie Cohen, Rob Lampe, and Se Hyeon Jang provided helpful comments on the manuscript. Funding for this project was provided to A.M., H.S. and S.G from the Center for Galápagos Studies (Office of the Vice Chancellor for Research) and the UNC College of Arts and Sciences, to E.N. by the Andrew Marion Blackmon family trust and a National Science Foundation grant to A.M. (OCE1751805).